

$$\nabla \cdot D = \rho_V$$

$$X(\omega) = \int_{-\infty}^{\infty} x(t) e^{-j\omega t} dt$$

$$\gamma = \alpha + j\beta$$

$$C = B \log_2 \left( 1 + \frac{S}{N} \right)$$

## Central Research Laboratory - Bangalore

केंद्रीय अनुसंधान प्रयोगशाला - बैंगलूरु

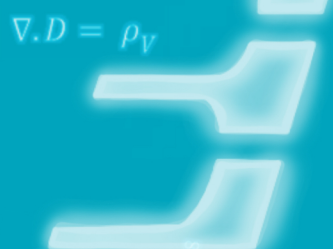
July 2023

जुलाई २०२३

$$\gamma = \alpha + j\beta$$

$$R_{max} = \sqrt[4]{\frac{P_S G^2 \lambda^2 \sigma}{P_{e_{min}} (4\pi)^3 L_{ges}}}$$

$$\beta = \frac{2\pi}{\lambda}$$



$$\nabla \cdot D = \rho_V$$

$$\nabla \times E = -\mu \frac{\partial H}{\partial t}$$

$$P_t = P_c \left( 1 + \frac{\mu^2}{2} \right)$$

$$f_s \geq 2f_m$$

$$C = B \log_2 \left( 1 + \frac{S}{N} \right)$$

$$\nabla \times H = J + \frac{\partial D}{\partial t}$$

$$\nabla \cdot H = 0$$

$$P = \frac{Z_L - Z_0}{Z_L + Z_0}$$

$$\beta = \frac{2\pi}{\lambda}$$

$$f(x) = \frac{1}{\sigma\sqrt{2\pi}} e^{-\frac{(x-a)^2}{2\sigma^2}}$$

$$E(x) = \int_{-\infty}^{\infty} x f(x) dx$$

$$\delta = \sqrt{\frac{2}{\omega \mu \sigma}}$$

$$P_R = \frac{P_t G_t G_r}{\left(\frac{4\pi R}{\lambda}\right)^2}$$

**BHARAT ELECTRONICS LIMITED**

**भारत इलेक्ट्रॉनिक्स लिमिटेड**

**[Ministry of Defence, Government of India]**

## Message from Chief Scientist

It gives me immense pleasure to note that the in-house journal of Central Research Laboratory LABTALK is back again. It is indeed heartening to note that advanced topics including fuel cells, Laser, OFDM etc. are being discussed in this June 2023 issue of LABTALK. No doubt, these papers represent the sample of futuristic research work being carried out at CRL. As Bharat Electronics stepping into new era of knowledge based professional electronics business, CRL has a very critical role to play to look into futuristic technologies.

In this regard LABTALK serves as a forum, sharing knowledge gained by experts in respective domain. I wish the LABTALK and its committee members huge success in bringing out the outcome of Research & Development by means of quality publications.

With Best Wishes,

L. Ramakrishnan,  
Patron, LABTALK,  
Central Research Laboratory,  
Bharat Electronics Limited,  
Bangalore.

## मुख्य वैज्ञानिक का संदेश

मुझे यह जानकर बेहद खुशी हो रही है कि केंद्रीय अनुसंधान प्रयोगशाला लैबटॉक की इन-हाउस पत्रिका फिर से आ रही है। यह वास्तव में दिल को छू लेने वाली बात है कि लैबटॉक के इस जून 2023 के अंक में ईंधन सेल, लेज़र, ओएफडीएम आदि सहित उन्नत विषयों पर चर्चा की जा रही है। इसमें कोई संदेह नहीं है कि ये पेपर सीआरएल में किए जा रहे भविष्य के अनुसंधान कार्यों के नमूने का प्रतिनिधित्व करते हैं। जैसे-जैसे भारत इलेक्ट्रॉनिक्स जान आधारित पेशेवर इलेक्ट्रॉनिक्स व्यवसाय के नए युग में कदम रखता है, सीआरएल की भविष्य की तकनीकों में देखने के लिए बहुत महत्वपूर्ण भूमिका है।

इस संबंध में लैबटॉक को संबंधित क्षेत्रों के विशेषज्ञों द्वारा प्राप्त जान को साझा करने के लिए एक मंच के रूप में कार्य करना चाहिए। मैं लैबटॉक और इसकी समिति के सदस्यों को गुणवत्तापूर्ण प्रकाशनों के माध्यम से अनुसंधान एवं विकास के परिणामों को सामने लाने में भारी सफलता की कामना करता हूं।

शुभकामनाओं के साथ

एल रामकृष्णन,  
संरक्षक, लैबटॉक,  
केंद्रीय अनुसंधान प्रयोगशाला,  
भारत इलेक्ट्रॉनिक्स लिमिटेड, बैंगलोर।

## Message from Editor

It gives me great pleasure to bring out the June 2023 issue of LABTALK. It contains 5 research papers covering futuristic research being carried out at CRL Bangalore for the indigenous BEL products. Fuel cells are one of the futuristic hopes for alleviating worlds energy crisis and the first paper discusses about cathode catalyst used in fuel cell. The research paper on fiber laser discusses about various design parameters for the 2 Kw CW fiber. The peak to average power ratio (PAPR) reduction in OFDM and the methods for computational complexity reductions are discussed in third paper. The fourth paper discusses the challenges faced to implement the secure socket shell (SSH) in custom ARM board. The paper on establishment of private wireless network using open-source software Magma discusses flexible open and extendable mobile core network. Apart from research papers the current issue contains technical writeup on the latest technology modules developed at CRL Bangalore and the recent granted patents.

On the behalf of editorial committee, I thank all the authors who have contributed to the current issue and also sincere gratitude to BEL Technical Literature Department for the print release of this issue of LABTALK and solicit continued cooperation in future also.

Dr. Viji Paul P.  
Editor, LABTALK,  
Central Research Laboratory,  
Bharat Electronics Limited, Bangalore

## संपादक का संदेश

मुझे लैबटॉक के जून 2023 के अंक को जारी करते हुए बहुत खुशी हो रही है। इसमें स्वदेशी बीईएल उत्पादों के लिए सीआरएल बैंगलूर में किए जा रहे भविष्य के अनुसंधान को शामिल करते हुए 5 अनुसंधान पत्र शामिल हैं। ईंधन सेल दुनिया के ऊर्जा संकट को कम करने के लिए भविष्य की उम्मीदों में से एक हैं और पहले पेपर में ईंधन सेल में उपयोग किए जाने वाले कैथोड उत्प्रेरक के बारे में चर्चा की गई है। फाइबर लेजर पर अनुसंधान पत्र में 2 किलोवाट सीडबल्यू फाइबर के विभिन्न डिज़ाइन मापदंडों के बारे में चर्चा की गई है। ओएफडीएम में पीक टू एवरेज पावर रेशो (पीएपीआर) की कमी और कम्प्यूटेशनल जटिलता में कमी के तरीकों पर तीसरे पेपर में चर्चा की गई है।

चौथे पेपर में कस्टम एआरएम बोर्ड में सुरक्षित सॉकेट शेल (एसएसएच) को लागू करने में आने वाली चुनौतियों पर चर्चा की गई है। ओपन-सोर्स सॉफ्टवेयर मैग्मा का उपयोग करते हुए निजी वायरलेस नेटवर्क की स्थापना पर पेपर में लचीले खुले और विस्तारणीय मोबाइल कोर नेटवर्क पर चर्चा की गई है। अनुसंधान पत्रों के अलावा वर्तमान मुद्दे में सीआरएल बैंगलूर में विकसित नवीनतम प्रौद्योगिकी मॉड्यूल और हाल ही में प्रदान किए गए पेटेंट पर तकनीकी लेखन शामिल हैं।

संपादकीय समिति की ओर से, मैं वर्तमान अंक के लिए योगदान देने वाले सभी लेखकों को धन्यवाद देता हूं और एलएबीटीएएलके इस अंक के प्रिंट रिलीज के लिए बीईएल तकनीकी साहित्य विभाग के प्रति आभार भी व्यक्त करता हूं और भविष्य में भी सहयोग जारी रखने का अनुरोध करता हूं।

डॉ. विजी पॉल पी.  
संपादक, लैबटॉक  
केंद्रीय अनुसंधान प्रयोगशाला,  
भारत इलेक्ट्रॉनिक्स लिमिटेड, बैंगलोर



## CONTENTS

Sl No.	Description	Page No.
<b>RESEARCH PAPERS</b>		
1	Solid-State Synthesis of Highly Dispersed and Efficient Pt/C Cathode Catalysts for Direct Methanol Fuel Cells <b>Author:</b> Basanta Kumar Roul	1
2	Design of 2kW CW Fiber Laser Source for D4 Systems <b>Authors:</b> Thejna Ros Joseph, Mahesh Lunavath, Renuka Sehgal and Ranu Tyagi	7
3	PAPR Reduction with Constellation Rotation and DFT-Precoded-OFDM <b>Authors:</b> Hari Krishna Boyapati, Rajeev Kumar Elubudi, Shashikant Chaudhari	13
4	Custom Secure Remote Management Module for MCT Switch <b>Authors:</b> Kunal Mohan Sadalkar	17
5	Establishment of Private Wireless Network Using Open-source Software Magma <b>Authors:</b> SoubhikBaral, Chaitanya P. Umbare, Jeevitha L, Nidhi Jain	21
<b>TECHNICAL WRITE UPS</b>		
1	SWIR imaging module for ADEOS-LR Contact Person: Karthick D	27
2	CPS MK II system for MBT Arjun Contact Persons: Nerella Arun Mani Kumar, Varanasi Krishna Priya	28
3	High Assurance Crypto System for Public Network Contact Persons: Jeevitha L, John Krishna Yaragorla, Hyndavi Rapuru, Rama Rao Ramisetty, Nidhi Jain	29
<b>GRANTED PATENT DETAILS</b>		
1	Systems and Methods for providing seamless communications and voice quality enhancement of VOIP	31
2	A method for Spectral and Temporal Measurements for Fiber Ring Laser	31
3	Device and Method for improved mode Decoding in Transponder system	32
4	A Method for Radar Bias Computation	32
5	A Method to Determine Cyclic Redundancy Check for a Multi Frame Data Word	33
<b>IMPORTANT EVENTS</b>		35-38
<b>LIST OF UPCOMING CONFERENCES</b>		



# Solid-State Synthesis of Highly Dispersed and Efficient Pt/C Cathode Catalysts for Direct Methanol Fuel Cells

Basanta Kumar Roul

Central Research Laboratory

Bharat Electronics Limited

Bangalore, India

Email: basanthkumarroul@bel.co.in

**Abstract-**To alleviate the world's current energy crisis, fuel cells play a significant role. The efficiency of a fuel cell primarily depends on the electrochemical catalytic activity of the catalysts used. Herein, we have synthesized a highly dispersed and efficient carbon-supported platinum-based cathode catalyst (Pt/C) with an excellent oxygen reduction reaction (ORR) for direct methanol fuel cell (DMFC) application. The 20 wt% Pt/C catalysts are synthesized using a solid-state process at different thermal decomposition temperatures of platinum(II)-acetylacetone (Pt(acac)<sub>2</sub>), where Pt(acac)<sub>2</sub> is used as a precursor for the production of platinum metal and Vulcan-carbon black is used as support material for platinum loading. The analysis of XRD and Raman spectroscopy confirmed that the Pt/C cathode catalyst synthesized at a thermal decomposition of 500 °C (Pt/C-500) has a higher crystallinity of platinum and lower degree of carbon graphitization, which are highly essential to promote a high ORR activity. In addition, the cyclic voltammetry analyses confirmed a lower onset potential and higher half-wave potential of ORR in the RDE polarization curve in Pt/C-500 catalyst along with long-term electrochemical durability as observed in the chronoamperometry curve. Furthermore, the peak power densities of single DMFC with Pt/C-500 are 82.28 and 92.87 mW/cm<sup>2</sup> at an oxygen backpressure of 0 and 10 psi, respectively, which are 95.9% and 101% higher than the commercial 40 wt% Pt/C. These results demonstrate that the Pt/C catalysts synthesized using the solid-state process have promising applications in DMFC.

## I. INTRODUCTION

A fuel cell is considered an emerging technology with great market potential and would be a source of energy for most of the applications in the future. Moreover, fuel cell plays a vital role in addressing the exhaustion of fossil fuels on the earth's crust. It is generally accepted that there are lots of advantages if fuel cells can be successfully commercialized. However, this is a demanding task to be accomplished, as there are some gaps in fuel cell technology itself which needs enhancement. It is believed that the high cost, less durability, and low efficiency of the fuel cells are the main limitations to be firstly overcome in enabling fuel cell technology to become viable for the market. Fuel cell technology is still evolving and there are some limitations and obstacles with the present level

of technology which are hindering the commercial exploitation of these fuel cells. Hence, it is vital to identify suitable fuel cell architectures and technologies for practical applications. Direct methanol fuel cell (DMFC) is considered to be the most emerging and promising fuel cell technology for most applications because of its low emission of pollutants, longer run times, short start-up time, low working temperature, simpler system architecture, etc. [1], [2]. In DMFC, methanol and oxygen are used as fuel and oxidants. Here, methanol is considered as an alternative and effective fuel because of its unique attributes, such as high specific energy density, low production cost, facile fuel storage, and ease of transport [3]–[5]. Despite many technological advantages of DMFC, there are drawbacks associated with DMFCs such as high material cost, methanol crossover from the anode to the cathode side, the slow kinetic reaction of methanol, low catalytic activity of the catalysts, low power density, low Pt utility efficiency of Pt/C catalysts, etc[6–10]. In addition, the loading of catalysts is considerably high in DMFC as compared to hydrogen-based proton exchange membrane fuel cell (PEMFC) due to the low catalytic activity of the catalysts, which severely cause charge-mass transfer limitation and hence further decreases the overall efficiency of DMFC[11].

In order to demonstrate an efficient DMFC, it is crucial to synthesize Pt/C catalysts with high catalytic activities by engineering their structure, morphology, and composition. Significant efforts have been made by different research groups to synthesize high-efficient and high-utility Pt/C cathode catalysts. To improve the Pt utility efficiency of Pt/C catalysts, researchers have focused on dispersing Pt metal on carbon black, thereby enabling an efficient DMFC. An effective dispersion method will not only result in a high Pt utility efficiency of Pt/C catalysts, but it will also reduce the quantity of Pt used. The synthesis techniques such as the hydrothermal[12], chemical-reduction[3,13,14], precipitation[15,16], solvothermal [17], impregnation-reduction[18, 19],etc, are widely used for the synthesis of dispersed Pt/C catalysts for fuel cell applications, where the yield of these techniques is very low. In addition, these techniques possess safety issues during the reaction process. All these limitations hinder the use of such synthesis techniques for commercial purposes, and hence a high-yield, safer synthesis technique should be used to synthesize high-efficient catalysts that are suitable for industrial-scale production. Mazzapoda et al.[17] have synthesized a mixture

of Pt/C and calcium-titanate ( $\text{CaTiO}_3$ ) using a solvo-thermal technique and demonstrated a single DMFC with a power density of  $\sim 68\text{mW/cm}^2$  at a cell temperature of  $60\text{ }^\circ\text{C}$ , where the enhanced ORR activity of Pt/C: $\text{CaTiO}_3$  is attributed to the presence of oxygen vacancies in  $\text{CaTiO}_3$ . Ghose *et al.*[3] prepared nitrogen-doped partially exfoliated carbon nanotube (PECNT) supported Pt-Ru (PtRu/PECNT) catalysts using ethylene glycol reduction method and fabricated a single DMFC. The cells exhibited a high-power density of  $\sim 67\text{ mW/cm}^2$  at an oxygen backpressure of 2 bar while operating at a cell temperature of  $60\text{ }^\circ\text{C}$ . The improved performance of DMFC is attributed to the superior electron-donating properties of CNT. In another report, Jha *et al.*[13] synthesized multi-walled carbon nanotubes (MWNTs) supported Pt (Pt/MWNT) and Pt-Ru (Pt-Ru/MWCT) catalysts using chemical-reduction method and demonstrated a single DMFC with a peak power density of  $\sim 29\text{mW/cm}^2$  at a cell temperature of  $60\text{ }^\circ\text{C}$ .

Herein, we have used a facile and high-yield solid-state process to synthesize a highly dispersed and efficient Pt/C cathode catalyst for DMFC application. The solid-state synthesis is an efficient and scalable process; hence this synthetic technique can be used on an industrial scale in the production of catalysts for fuel cells. Here,  $\sim 20\text{ wt\%}$  Pt on carbon black (Pt/C) cathode catalysts have been synthesized at different thermal decomposition temperatures of platinum (II)-acetylacetone ( $\text{Pt}(\text{acac})_2$ ), where  $\text{Pt}(\text{acac})_2$  is used as a precursor for the production of platinum metal and carbon black is used as support material for platinum loading. Moreover, a single DMFC has been fabricated using Pt/C as a cathode catalyst synthesized at  $500\text{ }^\circ\text{C}$ , which exhibits a high peak power density. This confirms that the Pt/C catalyst synthesized at  $500\text{ }^\circ\text{C}$  shows an efficient electrochemical activity as a cathode catalyst for ORR. The output peak power densities of single DMFC are  $82.28$  and  $92.87\text{ mW/cm}^2$  at an oxygen backpressure of 0 and 10 psi, respectively, operated at

## II. EXPERIMENTAL

### 2. 1. Synthesis of Pt/C catalysts

The synthesis of highly dispersed Pt/C catalysts was carried out using a solid-state process. Here, platinum(II)-acetylacetone( $\text{Pt}(\text{acac})_2$ ) was used as a precursor for platinum and carbon black (Vulcan XC-72R) was used as support material for platinum. The sequential procedures for the synthesis of the Pt/C catalyst are shown in **Figure 1**. Initially,  $\text{Pt}(\text{acac})_2$  precursor was mixed with acetone and stirred till the precursor completely dissolved to obtain a transparent solution. Subsequently, carbon black was added and then mixed ultrasonically for about 15 min followed by the magnetic stirrer for 1.5 h to obtain a homogeneous mixture of  $\text{Pt}(\text{acac})_2$  with carbon black. Afterward, the mixture was heated at a very low temperature to evaporate acetone from the mixture. Once the acetone was completely removed, the mixture was grinded using a mortar and pestle to make the mixture fine and disperse. Finally, highly dispersed Pt/C catalysts were obtained through the thermal decomposition of  $\text{Pt}(\text{acac})_2$  in a quartz tube furnace. Here, we have varied the thermal decomposition temperature of  $\text{Pt}(\text{acac})_2$  (we named as “synthesis temperature”) from  $300$  to  $600\text{ }^\circ\text{C}$  at an interval of  $100\text{ }^\circ\text{C}$ . The thermal decomposition was carried out for 4 h in presence of a continuous flow of argon gas with a flow rate of 120 sccm. Hereafter, the naming of the Pt/C catalysts synthesized at  $300$ ,  $400$ ,  $500$ , and  $600\text{ }^\circ\text{C}$  will be Pt/C-300, Pt/C-400, Pt/C-500, and Pt/C-600, respectively.

### 2. 2. Instruments and characterizations

Detailed structural and chemical characterizations have been performed for all the procured samples to get an insight into the chemical and physical behavior of catalyst materials that are attributed to the observed activity trend. The structural characterization of synthesized Pt/C catalysts was carried out using a PANalytical X-ray diffractometer (XRD) equipped with monochromatized  $\text{Cu K}\alpha$  radiation of  $1.54\text{ \AA}$

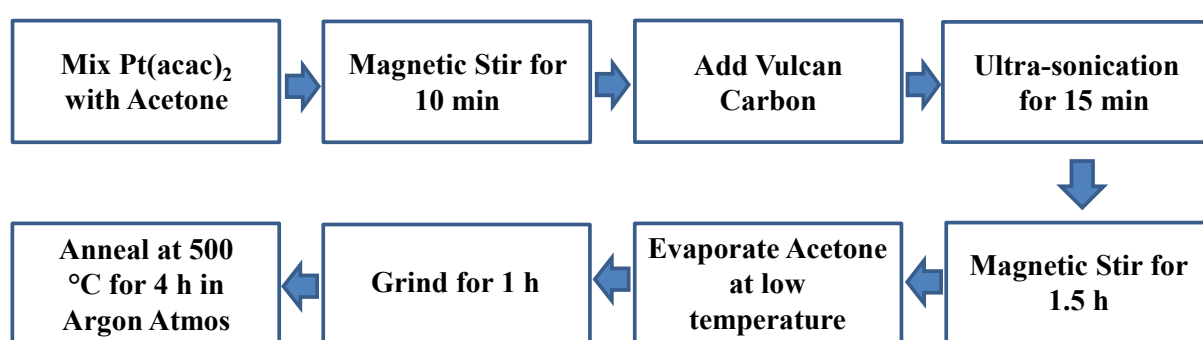


**Figure 1.** The sequential procedures for the synthesis of Pt/C-based catalysts using a solid-state process.

a cell temperature of  $60\text{ }^\circ\text{C}$ , which are  $95.9\%$  and  $101\%$  higher than the commercial  $40\text{ wt\%}$  Pt/C. These results demonstrate that the Pt/C catalysts synthesized using solid-state process have promising applications in DMFC.

wavelength source.

### 2. 3.Electrochemical measurements

The electrochemical measurements were performed on a three-electrode configured CHI 750E bipotentiostat based system where a glassy carbon electrode with a well-polished geometrical surface area of  $0.07\text{ cm}^2$  is used as the working electrode, Ag/AgCl is used as the reference and Pt wire as the counter electrode. Catalyst ink for the modified electrode preparation is made by dispersing about 7 mg of catalyst in a 1:1 water-ethanol mixture with a 20 percent addition of Nafion (5%) binder. The ink is sonicated well for 15 min and drop cast onto the glassy carbon electrode (GCE) surface and dried under infrared light to get the well-coated Pt/C modified electrodes which are used for further electrochemical measurements. The oxygen reduction reaction is measured in 0.5M  $\text{H}_2\text{SO}_4$  electrolytic solution.

10%)/C as an anode catalyst and in-house ~20% Pt/C as a cathode catalyst. The loading of anode and cathode catalysts on GDL was maintained at  $4\text{ mg/cm}^2$ , and the effective active area of the MEA was  $5\times 5\text{ cm}^2$  ( $25\text{ cm}^2$ ).

### 2. 5.Design and assembly of single DMFC.

Design of fuel flow patterns was carried out using SOLIDWORKS CAD tool. Herein, we have designed and fabricated a serpentine-cum-parallel flow pattern on a graphite plate for both methanol and oxygen flow, as shown in **Figure 2(b)**. **Figure 2(c)** shows an assembled fuel cell, where MEA, patterned graphite plates, rubber gaskets, current collector copper plates, and aluminium end plates were put together. Here, gaskets are used to prevent leakage of methanol and

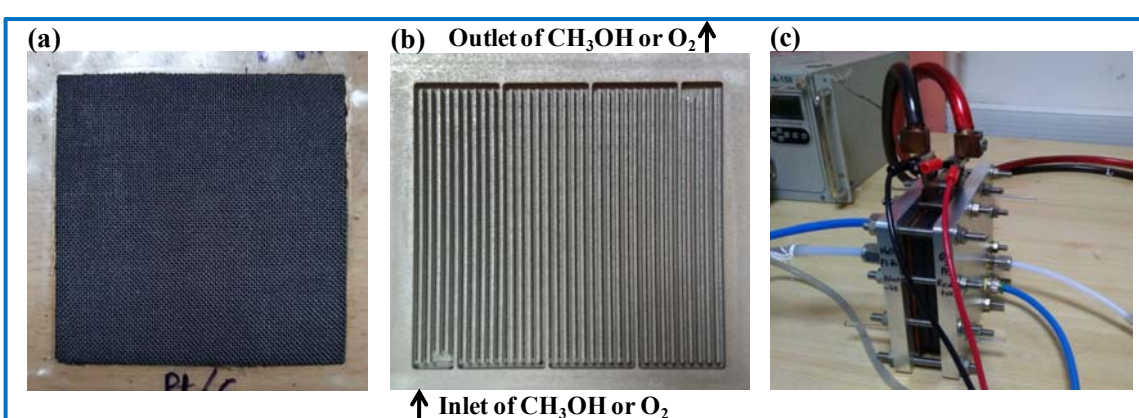


**Figure 2.**(a) Fabricated MEA with an active area of  $5\text{ cm}\times 5\text{ cm}$  ( $25\text{ cm}^2$ ). (b) The serpentine-cum-parallel flow pattern on graphite plate. (c) Assemble and test a fuel cell.

### 2. 4.Fabrication of membrane electrode assemblies (MEAs)

The primary components of MEA are gas diffusion layers (GDLs), catalyst layers, and the electrolyte membrane. The processes involved in the fabrication of MEAs are cleaning of the electrolyte membrane, preparation of catalyst ink, coating of catalyst ink on GDLs, and hot-press of electrolyte membrane with GDLs. Here, the commercial carbon cloth is used as GDL, and the Nafion-117 membrane was used as an electrolyte. Initially, the Nafion-117 membrane was boiled in 3%  $\text{H}_2\text{O}_2$  at  $100^\circ\text{C}$  for 1 h to remove unwanted organic impurities present in the membrane followed by rinsing with de-ionized (DI) water. Then, the membrane was boiled in DI water at  $120^\circ\text{C}$  for 1 h to remove excess peroxide. To make the membrane  $\text{H}^+$  ion conducting, the membrane was treated with 0.5M  $\text{H}_2\text{SO}_4$  solution at  $60^\circ\text{C}$  for 1 h and then boiled in DI water at  $120^\circ\text{C}$  for 1 h. To prepare the catalyst ink, the catalysts were mixed with Nafion<sup>®</sup>D-521 dispersion and ultra-sonicated for 40 minutes to obtain a homogeneous ink. Subsequently, the catalyst inks were coated on GDLs. Finally, the MEAs were fabricated by sandwiching Nafion-117 membrane with the catalyst-coated GDLs using a hot press at  $120^\circ\text{C}$  for 5 min under a pressure of  $\sim 35\text{ kg/cm}^2$  (**Figure 2a**). Here, we have taken commercial Ru-Pt (10%-

oxygen. Copper plates are used to collect the current, whereas aluminum end plates are used to hold the entire cell assembly.

## III. RESULTS AND DISCUSSION

**Figure 3(a)** shows the XRD pattern of Pt/C catalysts synthesized at different temperatures along with a commercial 40 wt% Pt/C catalyst. The diffraction peaks at  $2\theta = 39.63^\circ$ ,  $46.11^\circ$ ,  $67.64^\circ$ ,  $81.48^\circ$ , and  $86.39^\circ$  are associated with the (111), (200), (220), (311), and (222) planes of the face-centered cubic (fcc) crystal structure of Pt metal. The peak at  $2\theta = 24.56^\circ$  is associated with the (200) plane of carbon black. In order to examine the crystallinity of Pt, we have estimated the full width at half maximum (FWHM) of the diffraction peak associated with the (111) plane of Pt. **Figure 3(b)** shows the variation of FWHM of (111) reflection of Pt with the synthesis temperature along with the commercial Pt/C catalyst. It is observed that the Pt/C-500 has a low value of FWHM, which indicates a higher crystallinity of Pt nanoparticles. **Figure 3(c)** shows Raman spectroscopy of Pt/C catalysts synthesized at different temperatures. The peaks at  $1345$  and  $1590\text{ cm}^{-1}$  are assigned to the disorder D-band and graphitic G-band of carbon, respectively. The intensity ratio of disorder D-band to graphitic G-band of carbon ( $I_D/I_G$ ), which is used to probe the degree of graphitization of carbon, is

plotted as a function of synthesis temperature along with the commercial Pt/C in **Figure 3(d)**. It is evident that the Pt/C-500 has a higher  $I_D/I_G$  value, indicating a lower degree of graphitization. From XRD and Raman spectroscopy, it is observed that the Pt/C-500 has higher crystallinity of Pt nanoparticle and a lower degree of carbon graphitization, which are utmost essential for a high-performance fuel cell.

The oxygen reduction reaction (ORR) is the most important in fuel cells and battery devices[27, 28]. To evaluate the performance of the ORR over the modified Pt-based catalysts, CV is performed in  $N_2$  and  $O_2$  saturated 0.5 M  $H_2SO_4$  solution. The CV of the best-performing Pt/C-500

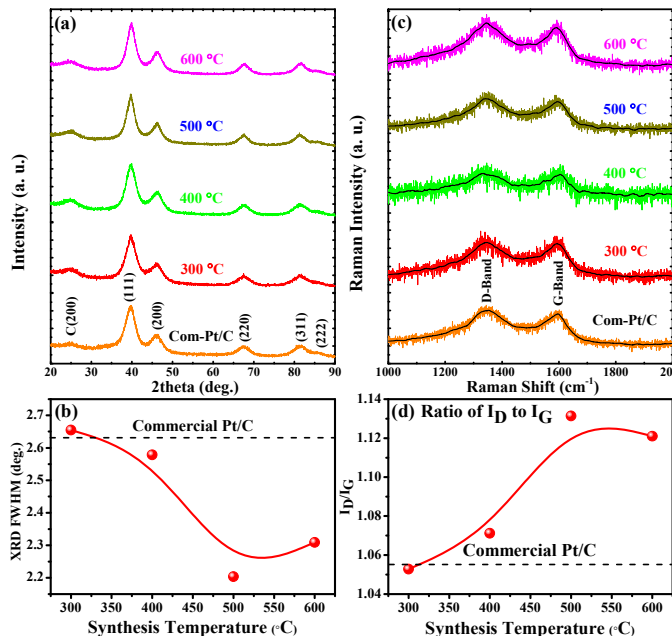


**Figure 3.** (a) XRD pattern of Pt/C catalysts synthesized at different temperatures along with commercial Pt/C catalyst, (b) the variation of FWHM of (111) reflection of Pt with the synthesis temperature along with the commercial Pt/C catalyst, (c) room temperature Raman spectroscopy of Pt/C catalysts synthesized at a different temperature, and (d) the intensity ratio of disorder D-band to graphitic G-band of carbon ( $I_D/I_G$ ) as a function of synthesis temperature along with the commercial Pt/C.

modified electrode is shown in **Figure 4(a)**. The recorded voltammogram displays a small reduction peak at 0.494 V in  $N_2$  saturated electrolyte solution which comes from the reduction of Pt-O surface[22]. Otherwise, the well-defined cathodic peak is observed at 0.491 V in  $O_2$  saturated electrolyte, confirming that the Pt/C-500 shows activity toward ORR. Further, the electro-catalytic activities of Pt/C-300, Pt/C-400, Pt/C-500, and Pt/C-600 for ORR are evaluated by linear sweep voltammetry curves recorded on an oxygen-saturated solution at 1600 rpm with the scan rate of 10 mV s<sup>-1</sup> and is shown in **Figure 4(b)**. Among all the catalysts, Pt/C-500 has an onset potential of 0.75 V compared with 0.62, 0.57, and 0.56 V for Pt/C-400, Pt/C-300, and Pt/C-600, respectively. However, the half-wave potential and the diffusion-limiting current densities are remarkably different from each other. The

half-wave potential of Pt/C-500 is 0.62 V, which is superior to all other Pt-based catalysts, and the diffusion limiting current density of -2.79 mA cm<sup>-2</sup> at 0.2 V which is lower than Pt/C-400 catalyst because of its slow kinetics at less positive potentials. To further investigate the ORR kinetics and the number of electron transfers involved in the ORR of Pt/C-500, LSVs are performed in  $O_2$  saturated 0.5 M  $H_2SO_4$  electrolyte solution using RDE at different rpms.

As illustrated in **Figure 4(c)**, the current density of the Pt/C-500 modified electrode increases with increasing the rpm. The K-L plots obtained by using the  $J^1$  value as a function of  $\omega^{-1/2}$  at different potentials are linear, indicating that the oxygen reduction reaction follows first-order reaction kinetics. The number of electrons involved in the reaction for Pt/C-500 was determined by using the K-L equation[23]. The Pt/C-500 catalyst exhibits good linear and parallelism modes of the plots (**Figure 4(d)**). Using the equation, the number of electrons transferred at Pt/C-500 is calculated to be ~3.94,

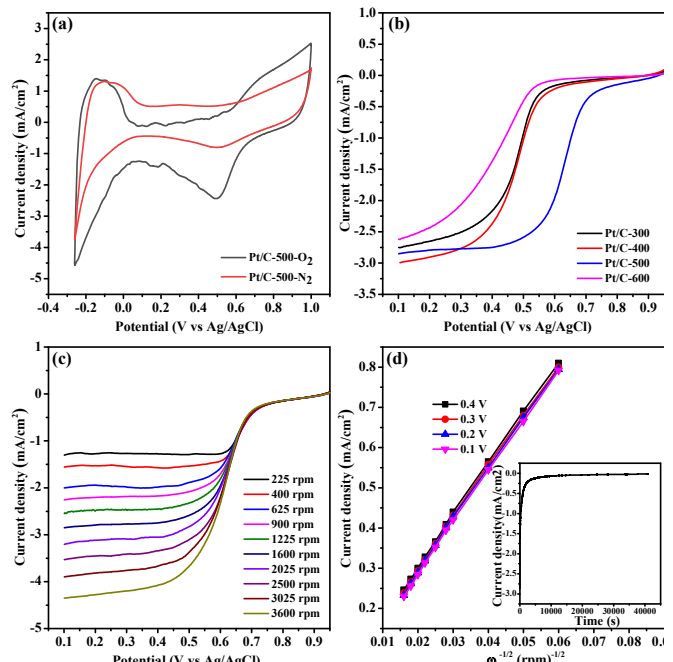


**Figure 4.**(a)CV curves of Pt/C-500 in  $N_2$ -saturated and  $O_2$ -saturated 0.5 M  $H_2SO_4$  solution with a sweep rate of 50 mV s<sup>-1</sup>, (b) LSV curves for Pt-based catalysts at an RDE rotation rate of 1600 rpm with a scan rate of 10 mVs<sup>-1</sup>, (c) RDE polarization curves of Pt/C-500 in  $O_2$ -saturated 0.5 M  $H_2SO_4$  solution with a sweep rate of 10 mV s<sup>-1</sup> at different rotating speeds ranging from 225 to 3600 rpm, and (d)The corresponding Koutecky-Levich plots ( $J^1$  vs  $\omega^{-1/2}$ )of Pt/C-500 at different potentials from 0.4 to 0.1 V from the polarization curves. Inset of (d) shows the stability test at an operating voltage of 0.55 V vs Ag/AgCl.

suggesting that the as-synthesized catalyst performs good ORR activity in acidic media. Chronoamperometry (CA) curves are often used to evaluate the durability of the catalysts[24]. The electrochemical durability of the Pt/C-500 catalyst is characterized by CA at 0.55 V in 0.5 M  $H_2SO_4$  solution, as shown in the inset of **Figure 4(d)**. Initially, the CA current decreased rapidly, and then the current density of

the catalyst became relatively stable. The rapid decrease in the initial current may be the charging current at the working electrode. At the initial stage of the CA measurement, the potential at the working electrode rapidly shifted to the set potential (0.55 V), which caused a charging current at the working electrode.

To examine the practical performance of Pt/C catalysts, the polarization curves of the fuel cells were carried out by measuring the output voltage of the cells at different load currents using a fuel cell workstation. During fuel cell measurements, the methanol and oxygen flow rates were maintained at 50 ml/min and 300 cc/min, respectively. The operating temperature of the fuel cell and concentration of methanol were fixed at 60 °C and 1.5 M, respectively. Here, the fuel cell measurements were carried out at oxygen backpressure of 0 and 10 psi at the cathode outlet. During the operation of the fuel cells, the water produced by the ORR at the cathode outlet was collected using a moisture trap. **Figures 5(a) and 5(b)** shows the polarization curves of the DMFCs

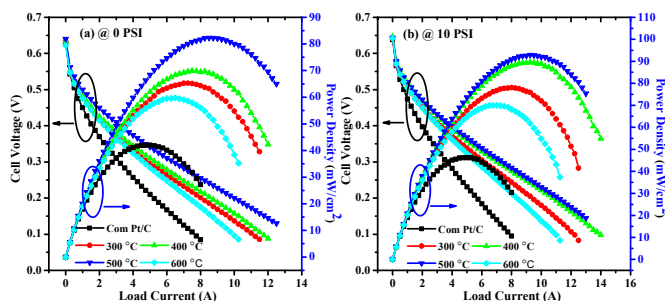


**Figure 5.** Polarization curves of the DMFCs at an oxygen pressure of (a) 0 PSI, and (b) 10 PSI with different MEAs. The MEAs are fabricated with in-house Pt/C as cathode catalysts that are synthesized at different temperatures.

measured at 0 and 10 psi oxygen backpressure applied at the cathode outlet, respectively. It is found that the cell voltage and peak power density of the cells at a particular load current are significantly influenced by the synthesis temperature of Pt/C catalysts. Here, the MEA with Pt/C-500 showed maximum cell voltage and highest peak power density at a particular applied load current. In addition, the MEA with Pt/C-500 catalyst showed maximum peak power densities of 82.28mW/cm<sup>2</sup> (at a current density of 352 mA/cm<sup>2</sup>) and 92.87 mW/cm<sup>2</sup>(at a current density of 380 mA/cm<sup>2</sup>) at an oxygen backpressure of 0 and 10 psi, respectively, which is 95.9% and 101% higher than the commercial 40 wt% Pt/C. Moreover, the MEA with Pt/C-500 catalyst showed the highest current density corresponding to the peak power density of DMFC among the four Pt/C catalysts. The above results demonstrate that the Pt/C catalysts synthesized by this solid-state process have promising applications in DMFC.

#### IV. CONCLUSION

In summary, we have synthesized highly dispersed and efficient 20 wt% Pt/C cathode catalysts with excellent ORR activity using a solid-state process at different synthetic

temperatures. The Pt/C catalyst synthesized at 500 °C (Pt/C-500) has a higher crystallinity of platinum and lower degree of carbon graphitization. The cyclic voltammetry analyses of Pt/C-500 confirmed a lower onset potential and higher half-wave potential of ORR in the RDE polarization curve along with long-term electrochemical durability as observed in the chronoamperometry curve. In addition, the output power density of a single DMFC with Pt/C-500 was 95.9% and 101% higher than commercial Pt/C at an oxygen backpressure of 0 and 10 psi, respectively.

#### REFERENCES

- [1] T. S. Zhao, C. Xu, R. Chen, and W. W. Yang, "Mass transport phenomena in direct methanol fuel cells," *Prog. Energy Combust. Sci.*, vol. 35, no. 3, pp. 275–292, 2009, doi: 10.1016/j.pecs.2009.01.001.
- [2] J. Larminie and A. Dicks, "Fuel cell systems explained: Second edition," *Fuel Cell Syst. Explain. Second Ed.*, pp. 1–406, 2013, doi: 10.1002/9781118878330.
- [3] A. Ghosh and S. Ramaprabhu, "An efficient and durable novel catalyst support with superior electron-donating properties and fuel diffusivity for a direct methanol fuel cell," *Catal. Sci. Technol.*, vol. 7, no. 21, pp. 5079–5091, 2017, doi: 10.1039/c7cy01522d.
- [4] Y. Cheng, C. Xu, P. K. Shen, and S. P. Jiang, "Effect of nitrogen-containing functionalization on the electrocatalytic activity of PtRu nanoparticles supported on carbon nanotubes for direct methanol fuel cells," *Appl. Catal. B Environ.*, vol. 158–159, pp. 140–149, 2014, doi: 10.1016/j.apcatb.2014.04.017.
- [5] X. Zhao *et al.*, "Recent advances in catalysts for direct methanol fuel cells," *Energy Environ. Sci.*, vol. 4, no. 8, pp. 2736–2753, 2011, doi: 10.1039/c1ee01307f.
- [6] S. S. Munjewar, S. B. Thombre, and R. K. Mallick, "Approaches to overcome the barrier issues of passive direct methanol fuel cell – Review," *Renew. Sustain. Energy Rev.*, vol. 67, pp. 1087–1104, 2017, doi: 10.1016/j.rser.2016.09.002.
- [7] H. Ahmad, S. K. Kamarudin, U. A. Hasran, and W. R. W. Daud, "A novel hybrid Nafion-PBI-ZP membrane for direct methanol fuel cells," *Int. J. Hydrogen Energy*, vol. 36, no. 22, pp. 14668–14677, 2011, doi: 10.1016/j.ijhydene.2011.08.044.
- [8] A. H. Tian, J. Y. Kim, J. Y. Shi, K. Lee, and K. Kim, "Surface-modified Nafion membrane by trioctylphosphine-stabilized palladium nanoparticles for DMFC applications," *J. Phys. Chem. Solids*, vol. 70, no. 8, pp. 1207–1212, 2009, doi: 10.1016/j.jpcs.2009.07.005.
- [9] A. Casalegno *et al.*, "Nanostructured Pd barrier for low methanol crossover DMFC," *Int. J. Hydrogen Energy*, vol. 39, no. 6, pp. 2801–2811, 2014, doi: 10.1016/j.ijhydene.2013.09.028.
- [10] S. H. Seo and C. S. Lee, "A study on the overall efficiency of direct methanol fuel cell by methanol

- crossover current," *Appl. Energy*, vol. 87, no. 8, pp. 2597–2604, 2010, doi: 10.1016/j.apenergy.2010.01.018.
- [11] S. Basu, "Recent trends in fuel cell science and technology," *Recent Trends Fuel Cell Sci. Technol.*, pp. 1–375, 2007, doi: 10.1007/978-0-387-68815-2.
- [12] M. Wang, K. Do Woo, and D. K. Kim, "Preparation of Pt nanoparticles on carbon nanotubes by hydrothermal method," *Energy Convers. Manag.*, vol. 47, no. 18–19, pp. 3235–3240, 2006, doi: 10.1016/j.enconman.2006.02.024.
- [13] N. Jha, A. Leela Mohana Reddy, M. M. Shaijumon, N. Rajalakshmi, and S. Ramaprabhu, "Pt-Ru/multi-walled carbon nanotubes as electrocatalysts for direct methanol fuel cell," *Int. J. Hydrogen Energy*, vol. 33, no. 1, pp. 427–433, 2008, doi: 10.1016/j.ijhydene.2007.07.064.
- [14] J. Lemus *et al.*, "Improved synthesis and hydrothermal stability of Pt/C catalysts based on size-controlled nanoparticles," *Catal. Sci. Technol.*, vol. 6, no. 13, pp. 5196–5206, 2016, doi: 10.1039/c6cy00403b.
- [15] A. K. K. Vikla *et al.*, "Tuning Pt characteristics on Pt/C catalyst for aqueous-phase reforming of biomass-derived oxygenates to bio-H<sub>2</sub>," *Appl. Catal. A Gen.*, vol. 610, no. November 2020, p. 117963, 2021, doi: 10.1016/j.apcata.2020.117963.
- [16] H. I. Joh, S. J. Seo, H. T. Kim, and S. H. Moon, "Preparation of Pt/C electrocatalysts using an incipient precipitation method," *Korean J. Chem. Eng.*, vol. 27, no. 1, pp. 45–48, 2010, doi: 10.1007/s11814-009-0320-6.
- [17] L. Mazzapoda, C. Lo Vecchio, A. S. Aricò, M. A. Navarra, and V. Baglio, "Performance improvement in direct methanol fuel cells by using CaTiO<sub>3</sub>-δ additive at the cathode," *Catalysts*, vol. 9, no. 12, 2019, doi: 10.3390/catal9121017.
- [18] B. Ruiz-Camacho *et al.*, "Oxygen reduction reaction on pt/C catalysts prepared by impregnation and liquid phase photo-deposition," *J. New Mater. Electrochem. Syst.*, vol. 13, no. 3, pp. 183–189, 2010.
- [19] C. Cao *et al.*, "Highly dispersed Pt/C catalysts prepared by the Charge Enhanced Dry Impregnation method," *Appl. Catal. B Environ.*, vol. 150–151, pp. 101–106, 2014, doi: 10.1016/j.apcatb.2013.12.004.
- [20] K. Kodama, T. Nagai, A. Kuwaki, R. Jinnouchi, and Y. Morimoto, "Challenges in applying highly active Pt-based nanostructured catalysts for oxygen reduction reactions to fuel cell vehicles," *Nat. Nanotechnol.*, vol. 16, no. 2, pp. 140–147, 2021, doi: 10.1038/s41565-020-00824-w.
- [21] R. Nandan *et al.*, "Atomic Arrangement Modulation in CoFe Nanoparticles Encapsulated in N-Doped Carbon Nanostructures for Efficient Oxygen Reduction Reaction," *ACS Appl. Mater. Interfaces*, vol. 13, no. 3, pp. 3771–3781, 2021, doi: 10.1021/acsami.0c16937.
- [22] Y. Huang, K. D. Seo, D. S. Park, H. Park, and Y. B. Shim, "Hydrogen Evolution and Oxygen Reduction Reactions in Acidic Media Catalyzed by Pd4S Decorated N/S Doped Carbon Derived from Pd Coordination Polymer," *Small*, vol. 17, no. 17, pp. 1–12, 2021, doi: 10.1002/smll.202007511.
- [23] M. Yeddala, D. B. Gorle, M. Anbu kulandainathan, P. Ragupathy, and V. K. Pillai, "Solid-state thermal exfoliation of graphite nano-fibers to edge-nitrogenized graphene nanosheets for oxygen reduction reaction," *J. Colloid Interface Sci.*, vol. 545, pp. 71–81, 2019, doi: 10.1016/j.jcis.2019.02.095.
- [24] H. Rachna Devi, O. Y. Bisen, X. Cao, Z. Chen, and K. K. Nanda, "Design of Hierarchical Oxide-Carbon Nanostructures for Trifunctional Electrocatalytic Applications," *Adv. Mater. Interfaces*, vol. 9, no. 14, pp. 1–17, 2022, doi: 10.1002/admi.202200071.



**Basanta Kumar Roul** received his M. Tech. degree in Solid State Materials from Indian Institute of Technology Delhi and Ph. D. degree in Materials Science from Indian Institute of Science, Bangalore, India. He is working as Member (Senior Research Staff) at Central Research Laboratory of Bharat Electronics Limited, Bangalore, India since 2005. His research activities and interests include epitaxial growth and characterizations of III-nitride semiconductors, thin films and nanostructures of polar and non-polar nitride semiconductors for optoelectronics applications.

# Design of 2kW CW Fiber Laser Source for D4 Systems

Thejna Ros Joseph, Mahesh Lunavath, Renuka Sehgal and Ranu Tyagi

EOL & EW Group

Central Research Laboratory, Bharat Electronics Limited

Bengaluru, India

Email: thejnaro@bel.co.in

**Abstract—** Drone Detect Deter and Damage (D4) systems tackle aerial drone threats using both soft-kill and laser based hard-kill. In this paper, we discuss the design of 2kW continuous-wave power ytterbium fiber laser to be used as an indigenous source for drone damage in D4 system. A 40W single oscillator fiber laser is the master oscillator, subsequently amplified by a bi-directional power amplifier stage. Optimization of design parameters to obtain required gain with suppressed nonlinearities is also investigated. Currently, indigenous development of 2kW laser sources based on this design is underway at BEL-PN to replace the imported laser source for D4 systems. The laser design along with the bill of materials is handed over to BEL-PN by CRL-BG.

**Index Terms ---** High Power Fiber Laser, D4 System, Bi-directional pumping, Master Oscillator Power Amplifier.

## I. INTRODUCTION

In recent times, drones have turned into an important concern for the defence forces. Owing to their easy availability, miscreants misuse unmanned drones to target, drop and supply weapons, explosives and ammunition during militant activities. Indian armed forces have inducted Drone Detect Deter and Damage (D4) systems designed by DRDO to tackle these aerial threats. D4 system is the first indigenously developed anti-drone system to neutralize enemy drone attacks by detection and soft-kill (jamming command and control units of micro drones) at a distance upto 3km and hard kill (laser based destruction of drones) upto 1.25km [1].

During hard kill, the laser engages, causing structural failure as it melts away the plastic housing and causing the drone's electronics to fail [2]. The range of the hard kill depends on the wattage of the laser used in the system. A continuous wave (CW) laser is required to accumulate heat to cause material damage. The laser power focused on the hostile drone, after incurring losses due to atmospheric propagation, should be sufficiently higher than its material damage threshold. Thus, the source laser is required to have high beam quality along with its high power. In a D4 system, to damage drones till 1.25km of range, the source laser needs to have a CW power of 2kW. This ensures that even after incurring losses during atmospheric transmission due to water molecules and other thermal phenomena, there will be sufficient power at the target to cause material damage. A beam director optics along with target tracking is also used to ensure that the laser beam is focused on the target until the target is damaged.

For generation of high laser power, fiber lasers are considered as the apt technological solution due to their high efficiency, excellent inherent beam quality, lack of alignment requirements and low thermal management. Ytterbium (Yb) doped fiber lasers can generate the required high power with 1μm wavelength. Along with easy availability of high power pumps, Yb doped fibers also have low quantum defect, thus, generating excellent efficiency and minimal heat even at high laser powers [3].

Worldwide, high power fiber lasers have seen significant advancements in terms of average powers in twenty first century. Zebiao Li et al realized a 2kW high-power counter-pumped all-fiberized laser without observation of thermal mode instabilities (TMIs) in 2017 [4]. A 2kW fiber laser with 20 m long delivery cable and high SRS suppression was reported by Y. Mashiko in Japan [5]. Wang et al demonstrated a laser system generated 2.04kW output power at 1080nm with 78.5% optical-to-optical efficiency with  $M^2 = 1.37$  [6]. Andrea Rosales-Garcia realized a monolithic 2.1kW single mode continuous wave fiber laser using 14/200μm double clad fiber amplifier in MOPA structure [7]. In China, a 2.43kW narrow linewidth linearly polarized all-fiber amplifier based on mode instability suppression using cylindrical spiral coiling of gain fiber was demonstrated in 2017 [8].

In this paper, we discuss the design of 2kW CW Yb fiber laser to be used as the indigenous laser source for hardkill in D4 system. In such sources, high laser power is confined within square-micrometer areas of optical fiber and this high optical intensity leads to nonlinear interactions of light with glass atoms. The resultant nonlinear phenomena can scatter power into undesired wavelengths and limit the power scaling. To obtain the high powers with reduced nonlinear effects such as Stimulated Raman Scattering (SRS) and Stimulated Brillouin Scattering (SBS), cladding pumped large mode area (LMA) fibers are used. For a given power, LMA fibers imply reduced optical intensities. Such fibers effectively exhibit weaker nonlinear effects and higher damage threshold. However, LMAs usually support a few higher order modes (HOMs) along with fundamental mode. Thus, a major obstacle in LMA fibers is the beam quality degradation due to the HOMs excitation and TMI. Design considerations to mitigate nonlinearities and TMI for 2kW power generation is also discussed in this paper.

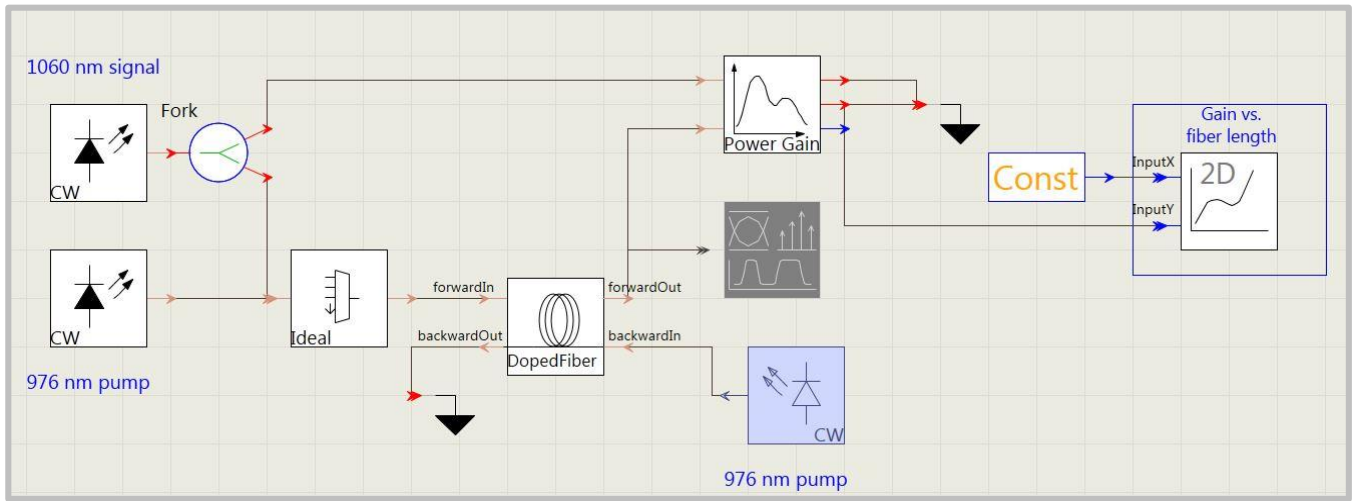


Fig. 1. Design setup for length optimizations of gain fibers using VPI software.

## II. DESIGN SIMULATIONS AND THEORETICAL ANALYSIS

In high power fiber laser sources, a master oscillator power amplifier (MOPA) configuration is used to amplify the low-power seed laser to meet the required power levels while preserving the spectral purity and beam quality. Various design parameters for the 2 kW CW fiber laser in MOPA configuration is analysed in below sections.

### A. Gain

As a result of meticulous experiments carried out over the years, the fiber laser community agrees upon the thumb rule for gain of amplifier stages to be 15dB. In case of oscillator this gain is 20dB [9]. For the 2kW fiber laser, thus the power amplifier stage can amplify a seed power of 40W to the required output. However, the coupling of seed power to power amplifier stage is limited by the availability high power handling isolators. Currently, commercial isolators upto 50W maximum power handling is available. An isolator is essential between the stages to avoid back reflections from amplifier stage from damaging the oscillator.

The effect of pumping configurations on mitigation of TMI and other nonlinearities is confirmed experimentally in [4]. Gain saturation has been proposed to increase TMI threshold. Different degrees of saturation break the symmetry between co-pumped and counter-pumped schemes. Notably, bi-directional pumping has higher threshold than co-pumping scheme. Fiber amplifier model including photodarkening effect indicated that a counter-propagating configuration had a higher TMI threshold. Other nonlinearities such as Stimulated Raman Scattering (SRS) and four wave mixing (FWM) are also suppressed in counter-pumping scheme. However, in our design we use bi-directional pumping for power amplifier stage. Semi-analytical model indicates the TMI threshold for bi-directional pumping to be 3.1kW for 15m of 20/400 $\mu$ m gain fiber. Bi-directional pumping creates optimal gain distribution, mitigating SRS and TMI through balanced reduction of peak nonlinear

phase and thermal gradients [10]. Moreover, in practice, thermal management of distributed pump load on the gain fiber in bi-directional pumping is easier to handle than that in the counter-pumping design. The unabsorbed pump load gets distributed among the cladding mode strippers (CMSs) on either sides of the gain fiber. The isolator in the design restricts the excess counter propagating pump after the CMS from damaging the oscillator stage.

### B. Pump wavelength

Minimization of gain fiber length is critical in increasing the nonlinearity threshold. Empirical data of absorption and emission cross-section of Yb ions in germanosilicate glass host reveals a sharp peak in absorption for pump wavelength of 976nm and a lower flatter peak around 915nm pump wavelength. Thus, pumping using 976nm instead of 915nm increases the pump absorption nearly 2.5 times, directly reducing the optimal length required. Moreover, the reduced quantum defect in this case, also improves the optical-to-optical efficiency with shorter fibers. However, when pumping with 976nm, TMI trends in the opposite direction, due to increased heat load and lower gain saturation [11]. The common tradeoffs needs to be balanced to deal with equally serious TMI and SRS. A optimized combination of pump diodes with and without wavelength stabilization can help in this cause. Inward pumping of the spirally coiled gain fiber with low bend radius can suppress the higher order mode and enhance TMI threshold [12]. Hence, power amplifier stage is bi-directionally pumped with 976nm pumps in this design.

### C. Fiber Length

Optimal length of gain fiber for both amplifier and oscillator stages are finalized using simulations. The rate equations for the quasi-three-energy-level structures are introduced with the relevant parameters in a beam propagation method algorithm to obtain the lasing power along the length of gain fiber.

Fig.1 shows the design setup for length optimizations of gain fiber using VPI software. The design setup shows a 1060nm seed laser and 976nm pump laser combined together using an ideal wavelength division multiplexer and pumped into Yb doped fiber. A 976nm pump laser was used to backward pump the gain fiber. The spectrum and gain versus fiber length trends are obtained using analyzer modules in the software. The results from the software were used to verify the custom simulations for

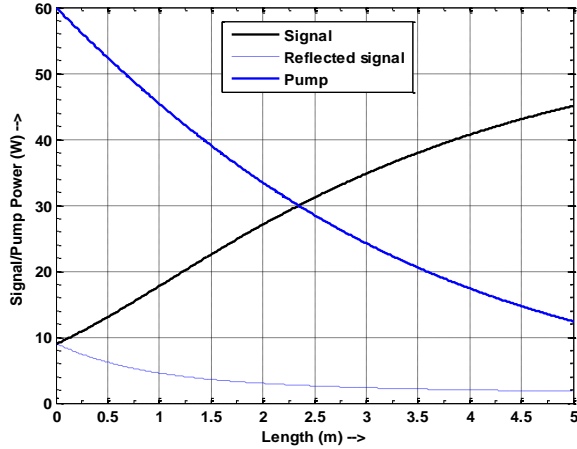


Fig. 2. Simulated output of the master oscillator.

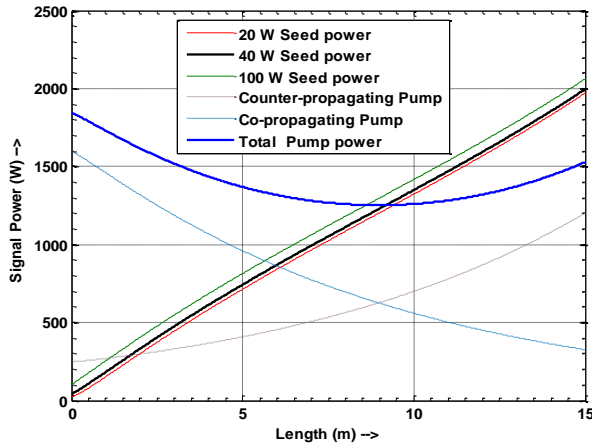


Fig. 3. Simulated output of the power amplifier.

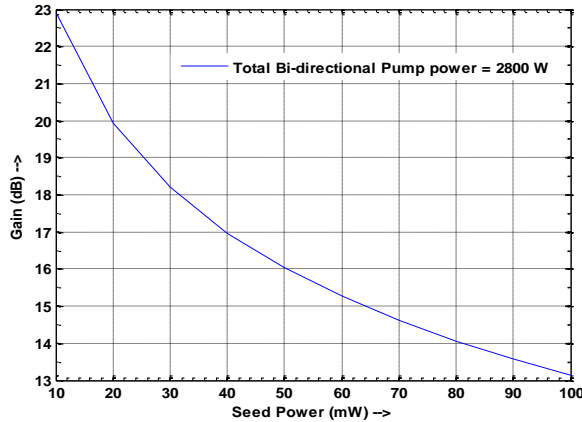


Fig. 4. Variation of power amplifier gain with seed power.

fiber laser and fiber amplifier configurations.

Fig.2 shows the simulated output of 10/130 $\mu$ m laser with 60W pump. 44W laser power is obtained with 5m long gain fiber. Power amplifier is simulated with 20/400 $\mu$ m fiber bi-directionally pumped with 1600W forward and 1200W backward propagating pump. Fig.3 shows 2kW laser power with 15m gain fiber length for 40W seed. The gain decreases with increase in seed power. 40W seed power extracts 17dB gain as seen in Fig.4.

ASE is also affected by the gain fiber length. ASE peak shifts to shorter (longer) wavelengths with shorter (longer) gain fiber length [13]. Further, the SRS threshold is inversely proportional to fiber length. With optimized length, ASE and nonlinearities are suppressed in the system.

#### D. SRS threshold

The threshold SRS nonlinearity in a fiber is defined as the incident power when the output Stokes light becomes equal to the remaining power of incident light. The SRS threshold power in fiber lasers is given by [14]:

$$P_{SRS} = \frac{16KA_{eff}}{g_R v_s L_{eff}}$$

Where  $P_{SRS}$  is the SRS threshold,  $K$  is the polarization factor, whose value between 0.5 and 1. When the laser beam maintain linear-polarization state, the value of  $K$  will be 0.5. And when the linear polarization states are chaotic, the value of  $K$  will be 1.  $A_{eff}$  is the effective mode area of the fiber,  $g_R$  is the Raman-gain coefficient and  $L_{eff}$  is the effective fiber length. For incident light of scrambled polarization,  $g_R$  is  $5 \times 10^{-14}$ . The theoretically calculated SRS threshold 20/400 $\mu$ m gain fiber with absorption coefficient of 1.25dB/m is 4.7kW . A gain fiber length of 15m, along with passive fiber length of 5m is considered. The use of LMA fibers for power amplifier stage is chosen to increase the effective mode area. As evident from the SRS threshold calculation, increasing the mode field area directly improves the SRS threshold. An important consequence of a large mode area is that the optical intensities for a given power level are low, reducing nonlinearities.

Appropriate thermal management is necessary to handle the residual heat. TMI threshold is also improved by actively cooling the gain fiber. Combination of demineralized water and monoethlyne glycol is used as coolant for the water chiller. Thermal management is of utmost importance in kW-class fiber lasers since the stability of the system is closely related to heat dissipation. In the simulations discussed in this paper, thermal simulations were not included.

### III. OPTICAL SYSTEM DESIGN

An all-fiberized MOPA optical engine design for the 2kW CW fiber laser is depicted in Fig.5. A master oscillator generating 40W laser CW power at 1064nm is used as the seed laser to a power amplifier stage separated by a 50W isolator.

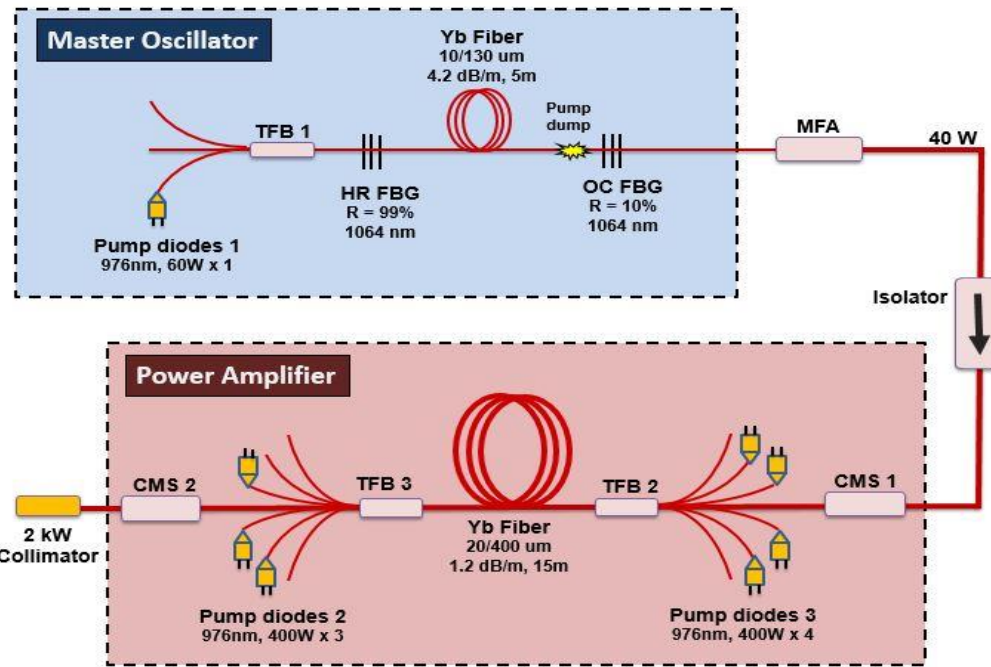


Fig. 5. Optical engine for 2 kW CW fiber laser.

In the seed laser, the laser resonator cavity is formed by Fiber Bragg Gratings (FBGs) pair with 1064nm central wavelength along with a 5m long gain medium. The gain medium is an Yb doped double cladding fiber (DCF) with core diameter of 10 $\mu\text{m}$  (numerical aperture (NA) = 0.06) and inner cladding diameter of 130 $\mu\text{m}$  (NA = 0.48). The absorption coefficient of the gain medium is 4.25dB/m at 976nm. The gain fiber is to be embedded in a spiral groove on the aluminum plate to provide better heatsinking. The gain fiber is inward pumped in this design. Inward pumping, the inner loop of the spiral groove is spliced to a HR-FBG. The HR-FBG has a reflectivity of 99.9% and the OC-FBG of 10% reflectivity. The pumping section of the seed laser is in co-pumping configuration. 60W of pump power at 976nm is combined of the pump diodes using a tapered fiber bundle (TFB). TFB1 has a power handling of 100W pump power with six 105/125 $\mu\text{m}$  (NA = 0.22) pump fiber inputs and one 10/130 $\mu\text{m}$  signal fiber input. The unused pump ports are flat cleaved and signal port is angle cleaved to minimize the back reflections back into the oscillator. This pumping configuration is expected to provide an output seed power of 40W with an optical-to-optical efficiency of 70%. The length of gain fiber is optimized through theoretical analysis. The unused pump after the gain fiber is dumped using a pumpdump.

The power amplifier stage is designed to amplify 40W of seed power into 2kW output with 17dB gain. This stage is designed using large mode area fibers to handle high powers with suppressed nonlinearities. A MFA is used after the master oscillator stage to match the mode field diameter of the seed output to large mode area dimensions. A high power handling isolator is used between the stages to protect the master oscillator stage from back-reflections of power amplifier. Currently, isolator technology is still evolving to be able to

handle high powers. High power isolators at 10/130 $\mu\text{m}$  can handle power much stabler than large mode area isolators.

The power amplifier stage is designed to be with bi-directional pumping. The large mode area fibers with core and inner cladding diameter of 20 $\mu\text{m}$  (NA = 0.06) and 400 $\mu\text{m}$  (NA = 0.46) respectively is used in this stage. The Yb doped gain fiber has an peak pump absorption coefficient of 1dB/m. It is bi-directionally pumped using a combination of forward (TFB2) and reverse TFB (TFB3). The (6x1)+1 TFB1 has power handling of 1kW for the seed port and 1.4kW for the six pump ports. TFB2 with 3.5kW power handling of seed port and 1.5kW pump power handling is used to counter pump. The seed port of TFB3 is handling the amplified 2kW laser power out the power amplifier stage. The power amplifier stage is pumped from either side using three 400W laser diodes each lasing at 976nm. This multimode lasers have fiber pigtails with 200/220 $\mu\text{m}$ . The unused pump ports needs are flat cleaved. The unabsorbed pump power is dumped using CMSs on either side of the gain fiber. Two CMSs with power stripping capacity of 300W each is used. A 5m water cooled delivery cable with 5kW power handling is used to deliver the 2kW laser power.

#### IV. CONCLUSION

In conclusion, we designed a 2kW CW fiber laser in MOPA configuration at 1064nm to be used for hard-kill in D4 systems. The master oscillator is a 40W fiber laser which is further amplified to 2kW by LMA amplifier stage. The seed power is limited by the current availability of commercial high power isolators. 40W seed can provide 17dB gain in a bi-directionally pumped 15m power amplifier. The gain fiber lengths and input seed power in the design is optimized according to the simulation results. Various fiber

building techniques to be incorporated to circumvent TMI, ASE and SRS are also discussed.

This fiber laser design will successfully meet the laser source requirements in D4 systems. BEL-PN has received STPO from BEL-MC to indigenize the laser source of D4 systems. Currently, Indigenous 2kW laser source development for D4 systems based on the design shared by CRL-BG, is being carried out at BEL-PN. This in-house developed fiber laser system is designed to directly replace the imported 2 kW laser source from foreign manufacturer (IPG Photonics).

## REFERENCES

- [1] "New counter drone system by DRDO can detect and eliminate aerial targets," Economics Times News, June 2021.
- [2] GCRK Narang, "Counter Drone Systems, An Opportunity for Self-Reliance," India Foundation, September 2021.
- [3] H. M. Pask, Robert J. Carman, David C. Hanna, Anne C. Tropper, "Ytterbium-Doped Silica Fiber Lasers: Versatile Sources for the 1-1.2  $\mu$ m Region" *IEEE Journal of Selected Topics in Quantum Electronics*, vol. 1, no. 1, April 1995.
- [4] Zebiao Li, Zhihua Huang et al, "Experimental demonstration of transverse mode instability enhancement by a counter-pumped scheme in a 2 kW all-fiberized laser," in *Photonics Research*, vol.5, no.2, pp. 77-81, April 2017.
- [5] Y. Mashiko, H. K. Nguyen et al, "2 kW single-mode fiber laser with 20-m long delivery fiber and high SRS suppression," in *Proc. of SPIE*, vol. 9728, no.3, March 2015.
- [6] Wang Wenliang, Huang Liangjin, Kong Lingchao, Guo Shaofeng and Jiang Zongfu, "2 kW CW near single mode all-fiber Ytterbium-doped fiber laser," in *Optik – International Journal for Light and Electron Optics*, May 2015.
- [7] Andrea Rosales-Gracia, Hideaki Tobioka, Kazi Abedin et al, "2.1 kW single mode continuous wave monolithic fiber laser," in *Proc. of SPIE*, vol. 9344, March 2015.
- [8] Rongtao Su, Rumao Tao, Xiaolin Wang et al, "2.43 kW narrow linewidth linearly polarized all-fiber amplifier based on mode instability suppression," in *Laser Physics Letters*, vol. 14, July 2017.
- [9] Optical Fiber FAQs, nLIGHT.Inc.
- [10] Pascal Deladurantaye, "SRS remains a major development challenge for multikilowatt fiber lasers used in industrial applications," in *Laser Focus World Magazine*, May 2021.
- [11] C. Jauregui, C. Stihler, J. Limpert, "Transverse Mode Instability," in *Advances in Optics and Photonics*, vol. 12, no.2, pp 429-484, 2020.
- [12] Thejna Ros, Mahesh Lunavath, Renuka Sehgal, Ranu Tyagi, " Field Portable 400 W CW Fiber Laser Source for Ordnance Disposal," *IEEE CONNECT*, July 2021.
- [13] Thejna Ros, Mahesh Lunavath, Ranu Tyagi, " 1kW Narrow-linewidth CW Fiber Laser Source for Spectral Beam Combining," *CRL Technical Symposium*, August 2022.
- [14] Jay.W.Dawson, Micheal J. Messerly, Raymond J. Beach et al, "Analysis of the scalability of diffraction-limited fiber lasers and amplifiers to high average power," in *Optics Express*, vol.16, no.17, August 2008.
- [15] Yong Wang, "Stimulated Raman Scattering in high-power double-clad fiber lasers and power amplifiers," in *Proc. of SPIE*, vol. 44(11), November 2005.

## BIO DATA OF AUTHORS



**Thejna Ros Joseph** received B.Tech degree in engineering physics from National Institute of Technology, Calicut in 2015 and the M.Tech degree in electrical engineering with photonics specialization from Indian Institute of Technology, Madras in 2017. She is currently working as Member Research Staff (MRS) in Central Research Laboratory, Bharat Electronics Limited, Bangalore. Her research interest are in fiber lasers, microwave photonics, computational electromagnetics and quantum key distribution.



**Mahesh Lunavath** received B.Tech degree in electrical engineering from Indian Institute of Technology, Roorkee, in 2014 and the M.Tech degree in electrical engineering with photonics specialization from Indian Institute of Technology, Madras in 2017. He is currently working as Member Research Staff (MRS) in Central Research Laboratory, Bharat Electronics Limited, Bangalore. His research interest includes high-power fiber lasers, microwave photonics and optical communications.



**Renuka Sehgal** received M.Sc., Physics degree from Kumaun University, Nainital in 2005 and M.Tech in Laser Science and its Applications from DAVV Indore in 2007. She is currently working as a Manager in Centre of Excellance – Electronic Warfare & Photonics, Bharat Electronics Ltd., Bangalore. Her areas of research interest are solid state lasers, Fiber Lasers and Laser Communication.



**Ranu Tyagi** received M.Sc., Physics degree from IIT Delhi in 1999 and M. Tech in Instrument Technology from IIT Delhi in 2001. She joined Central Research Laboratory of Bharat Electronics Ltd., Bangalore in 2001 and currently working there as a Member Senior Research Staff (SRS). Her current areas of research interest are High Power Fiber Lasers, MEMS, Fiber Optic Sensors, Inertial Navigation Systems and microwave photonics.

\*\*\*



# PAPR Reduction with Constellation Rotation and DFT-Precoded-OFDM

Hari Krishna Boyapati (MRS)  
Wireless Networks,  
CRL-BEL, Bangalore, India.  
harikrishnaboyapati@bel.co.in

Rajeev Kumar Elubudi (MSRS)  
Wireless Networks,  
CRL-BEL, Bangalore, India.  
rajeevkumarelubudi@bel.co.in

Shashikant Chaudhari (MSRS)  
Wireless Networks,  
CRL-BEL, Bangalore, India.  
cshashikantyeshwant@bel.co.in

**Abstract**—In this paper, peak-to-average power ratio (PAPR) problem of OFDM based waveforms is considered with the transmission of  $\pi/4$  rotated QPSK,  $\pi/2$  rotated BPSK modulations and DFT precoded OFDM. 10 MHz waveform is considered. The realization of DFT-precoded -OFDM requires M-point DFT/IDFT implementation. If, M is non-power of two, Computational complexity of the implementation of DFT/IDFT with two different methods such as split FFT and matrix based approach has been analyzed. The proposed combination of constellation rotated modulations and DFT-S-OFDM has significant improvement of PAPR and also computationally less complex with matrix based approach when compared to plain CP-OFDM.

**Keywords**—DFT-S-OFDM,  $\pi/2$  – BPSK,  $\pi/4$ - QPSK

## I. INTRODUCTION

The Orthogonal Frequency Division Multiple Access (OFDMA) is being used in all the current and next generation wireless standards to efficiently use the operating frequency band in spectrum and also provide high data rates. In addition, large numbers of antennas are added to base station side to increase the coverage. Multiple spatial layers of processing are used on top of this to further achieving the Giga bit data rates in wireless. Common core multi carrier waveform in all these technologies is OFDMA.

The biggest problem with OFDM waveform is its high peak-to-average power ratio (PAPR). This is due to non linear peaks produced as a result of summing the multiple carriers at the output of the digital baseband processing. This in turn carried by Radio front end with power amplifiers in a specific frequency band. As shown in figure-1, the input-output characteristics of power amplifier represent the non-linear characteristics. Peaks preset in the waveform input are severely degraded at the PA output, when it passes through non-linear region. Hence, the design of RF power amplifier becomes more difficult when it handles high PAPR waveform because of following:

- Output signal of PA will be distorted and distortion of the signal depends on the PA operation point.
- If PA operated in linear region PA efficiency will be less.
- Back-off can be applied before PA to reduce output power and there by operating in linear region.

However, it reduces the transmission power and hence coverage area.

- Spectral regrowth occurs due to inter modulation product components created at the output of PA.
- This in turn causes Block Error Rate (BLER) degradation and Adjacent Channel Interference (ACI).

Hence, methods for reducing PAPR are very much needed to improve the efficiency of the PA by pushing the operating point further.

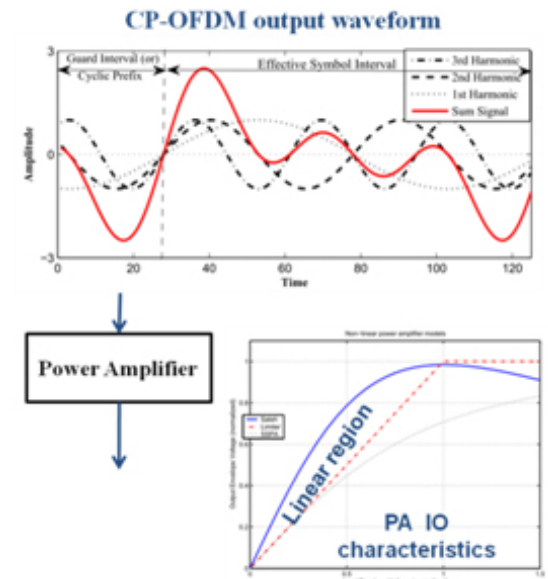


Figure-1: PAPR problem at PA output

Reducing the PAPR will help the PA to operate with less non linear distortion and reduces both the in-band (IB) and out-of-band (OOB) distortions. This leads to meeting the tight adjacent channel rejection ratio (ACLR) requirements. 3.5G to 5G, 3gpp standards has adopted OFDMA in the downlink and discrete Fourier transform-precoded-OFDMA (DFT-precoded-OFDMA) [1] (also known as single-carrier frequency-division multiple access (SCFDMA)) in the uplink. The main advantage of SCFDMA waveform is lower PAPR, which results in less power amplifier back-off compared with OFDMA. This in turn increases the range of communication. SC-FDMA applies DFT precoding on the baseband modulation symbols before transmitting the data on the subcarriers.

To enhance the cell coverage of OFDM systems further, reducing the PAPR with constellation rotated modulation schemes, namely  $\pi/2$ -BPSK and  $\pi/4$ -QPSK were explored. These schemes exhibit a much smaller peak-to-average power ratio (PAPR) of the transmitted signal than the QPSK and higher-order modulations do [2]. It is also proven that constellation rotation on higher order modulations will increase the complexity of decoding with minimal improvement on PAPR. Consequently, these modulations increase the cell-edge connectivity. In this paper, combination of  $\pi/2$  and  $\pi/4$  rotated constellation on modulations along with DFT-spread OFDM has been simulated in matlab for PAPR reduction. Implementation complexity of N-point FFT when  $N$  is non power of two has been assessed in two approaches.

The rest of the paper is organized as follows. Section-II will describe the Complementary Cumulative Distribution Function of PAPR In section-III, DFT-spread-OFDM modulation in detail. In section-IV, Constellation rotation explained. In section-V, proposed functional block diagram of rotated constellations on modulations and their PAPR results are given. A comparison is done on computational complexity of N-point DFT implementation, when  $N$  is non power of 2. Finally Section-Vi and VII summary and future work are given.

## II. CCDF OF PAPR

PAPR definition [3]: PAPR is the ratio between the maximum power and the average power of the complex pass-band signal set), it can be defined mathematically as

$$\text{PAPR} = \frac{\max_{0 < t < T} |s(t)|^2}{E[|s(t)|^2]}$$

Amplitude is considered instead of power then the parameter is called as crest factor (CF).

$$\text{Crest Factor} = \sqrt{\text{PAPR}}$$

In the OFDM system with multiple subcarriers, the maximum peak power occurs when all of them are added with identical phases. In general in hostile wireless channel the largest PAPR rarely occurs. Thus, finding the probability that the pass band signal power is out of the linear range of the HPA is important parameter. Cumulative distribution function does this function of finding probability that PAPR of a randomly generated  $N$ -carrier OFDM symbol less than or equal to PAPR threshold. Contrast to that, Complementary CDF (CCDF) defines the probability that the PAPR exceeds PAPR threshold (i.e. below which HPA can be operated in linear range). CCDF of PAPR [4, 5], which is given as

$$\text{CCDF of PAPR} = 1 - \text{CDF of PAPR}$$

CCDF expected to be as low as possible for any waveform. It gives the measure of probability of power level of peak crosses its average power value.

## III. DFT precoded OFDM

In DFT precoded OFDM (or) SC-FDMA, the  $M$ -point DFT is applied on subcarriers before subcarrier mapping and IFFT. This operation results in each subcarrier after the IFFT will contain part of each symbol. Hence, SCFDMA presents the benefit of a single carrier multiplexing of having a lower Peak-to-average Power Ratio. Because of this low PAPR advantage, current 4G and 5G standards use SCFDMA on the uplink. The difference between SC-FDMA and OFDMA has been shown in figure-2. The symbols are mapped on separate carriers in OFDMA, where each symbol is mapped on all the subcarriers in the case of SCFDMA. This means in SCFDMA, all subcarriers on a period of time represent the same symbol.

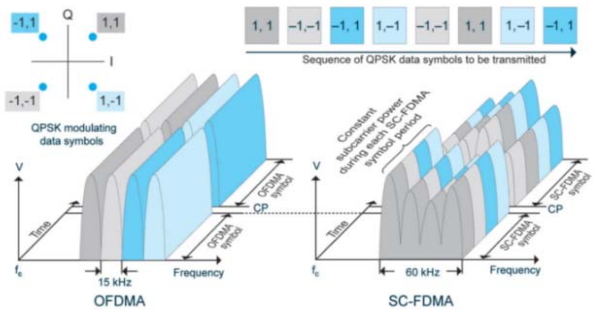


Figure-2: Frequency vs. Time representation of QPSK symbols mapped to subcarriers in OFDMA and SCFDMA [6].

## IV. CONSTELLATION ROTATION ON MODULATION

Constellation rotation avoids zero crossings, which means that the symbol to symbol amplitude variations are low and further it avoids the non uniform peak variations from symbol to symbol.  $\pi/2$  BPSK,  $\pi/4$  QPSK are two low complexity constellation rotated modulations which results in low peak variations.

### a) $\pi/2$ BPSK:

In  $\pi/2$  BPSK, even and odd bit positions are divided into two sets of BPSK constellations that are shifted by  $90^\circ$ . These sets are selected depending on the position of the bits in the input sequence.  $\pi/2$  BPSK and BPSK modulation symbols are defined as per Equation (1), Equation (2) [6].

$$d(i) = e^{j(i \bmod 2)\frac{\pi}{2}} \left\{ \frac{1}{\sqrt{2}}(1 - 2b(i)) + j(1 - 2b(i)) \right\} \quad (1)$$

$$d(i) = \left\{ \frac{1}{\sqrt{2}}(1 - 2b(i)) + j(1 - 2b(i)) \right\} \quad (2)$$

$b(i)$  = input bits;  $i$  = position or index of input bits;  
 $d(i)$  = mapped bits (constellation points)

Figure-3 shows the ideal constellations and waveforms for BPSK and  $\pi/2$  BPSK, when long sequences of random input bits are input to the BPSK and  $\pi/2$  BPSK modulators respectively. From the waveform,  $\pi/2$  BPSK has more phase transitions than BPSK. Therefore  $\pi/2$  BPSK also helps in better synchronization, especially for cases with long runs of 1s and 0s in the input sequence.

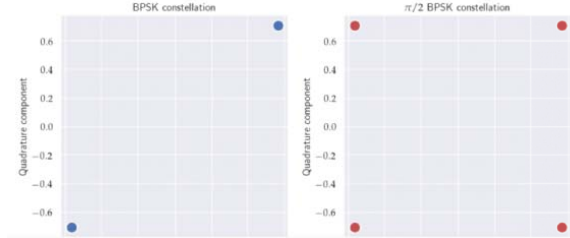


Figure-3: Constellations of BPSK and  $\pi/2$  BPSK modulations

Following is the example output of  $\pi/2$  BPSK modulation for the given bit stream.

Bitstream: 1 0 1 1 0 1 1 0 0 1

Even position bits: 0 1 1 0 1

Odd position bits: 1 1 0 1 0

From equations (1) and (2), even position and odd position bits are mapped to constellation points given in Table-I. Total four constellation points. Figure-4 shows the simulated result of  $\pi/2$  BPSK.

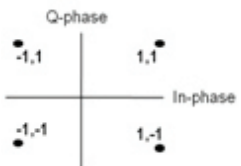


Figure-4:  $\pi/2$  BPSK Constellation and  $\pi/2$  BPSK constellation mappings for input bit stream

#### b) $\pi/4$ QPSK:

$\pi/4$  QPSK uses two sets of QPSK constellations that are shifted by  $90^\circ$ . The constellation is having two sets of QPSK constellations. The first set is normal QPSK and second set is  $\pi/4$  shifted version of QPSK. Here also similar to  $\pi/2$  BPSK, the constellations sets are selected depending on the position of the bits (i.e. even or odd) in the input sequence. Figure shows the  $\pi/4$  rotated constellation of QPSK.

Following is the example output of  $\pi/4$  QPSK modulation for the given bit stream.

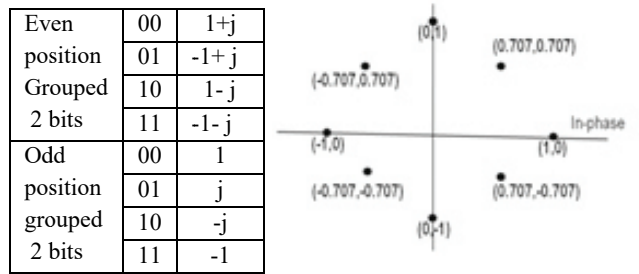


Figure-5:  $\pi/4$  QPSK Constellation and  $\pi/4$  QPSK constellation mappings for input bit stream

Bit stream: 1 0 1 1 0 1 1 0 0 1 1 0 1 1 0 1 1 0 0 1

Even position bit group: 10, 01, 01, 11, 10,

Odd position bit group: 11, 10, 10, 01, 01

Similar to  $\pi/2$  BPSK, in  $\pi/4$  QPSK the even position and odd position bit groups are mapped to constellation points given in Table-II. Total eight constellation points are there in  $\pi/4$  QPSK. The added advantage of this modulation is, it will provide the same data rate as plain BPSK with reduced PAPR. The same analysis applied to  $\pi/4$  QPSK also.

## V. PROPOSED COMBINED ARCHITECTURE

The top-level architecture of constellation rotated modulation along with DFT-precoded-OFDM transmitter is shown in figure-6(a) and figure-6(b).

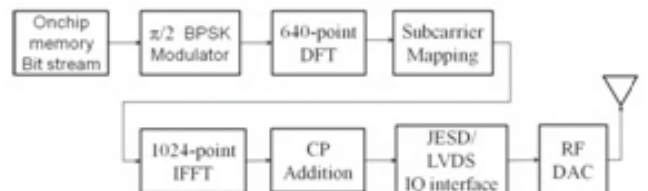


Figure-6(a):  $\pi/2$  BPSK and SCFDMA transmitter blocks

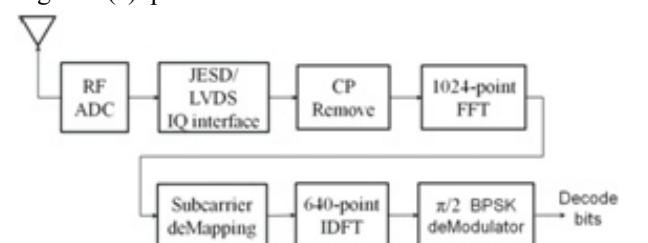


Figure-6(b):  $\pi/2$  BPSK and SCFDMA receiver blocks

A waveform with bandwidth of 10 MHz is considered, the pre DFT length is chosen as 640 and IFFT length is chosen as 1024. These values are deviation from LTE specification to increase the number of data carriers. The implementation of 640-point FFT/IFFT, there is no IP core present from Xilinx or Altera, as this block is non-power of two. Hence, this block has to be implemented using either of following two approaches [7]. Split FFT approach and Matrix based FFT approach.

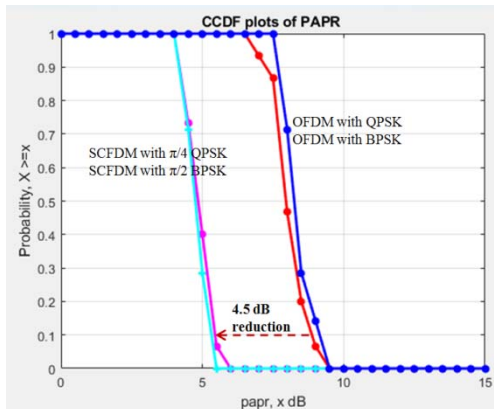


Figure-7: Simulated output CP-OFDM with plain modulations and SCFDM with rotated constellations

First approach requires normalization on output values after computing all the partially computed FFTs. This approach computation complexity is more and matrix based approach computationally less complex and saves the hardware resources. Hence, the computationally efficient matrix based FFT computation has been chosen for development. The hardware resource comparison is given in Table-III for both approaches. The 640-point DFT/IDFT is considered for example. It can be factorized into  $M=128$ ,  $L=5$ .

TABLE-III: COMPUTATIONAL COMPLEXITY

Parameter	Split Approach $N=640$ , $M=128$ , $L=5$ ( $N=ML$ )	Matrix Approach
Number of Complex Multipliers	$N^2$	$N*(M+L+1)$
Number of Complex Additions	$N^2$	$N*(M+L-2)$

## VI. SUMMARY AND CONCLUSION

The  $\pi/2$  constellation rotation on BPSK and  $\pi/4$  rotation on QPSK along with the DFT-precoded OFDM simulated in Matlab. This combination will have 4 to 5 dB PAPR reductions. The simulated result is given in figure-7. The implementation complexity of 640-point DFT/IDFT has been analyzed and presented in this paper.

## REFERENCES

- [1] J. Kim, Y. H. Yun, C. Kim and J. H. Cho, "Minimization of PAPR for DFT-Spread OFDM With BPSK Symbols," in IEEE Transactions on Vehicular Technology, vol. 67, no. 12, pp. 11746-11758, Dec. 2018, doi: 10.1109/TVT.2018.2874688.
- [2] J. Kim, Y. H. Yun, C. Kim and J. H. Cho, "A Further PAPR Reduction for  $\pi/2$ -BPSK in 5G New Radio," 2018 IEEE 88th Vehicular Technology Conference (VTC-Fall), Chicago, IL, USA, 2018, pp. 1-5, doi: 10.1109/VTCFall.2018.8690859.
- [3] Hideki Ochiai, "On the Distribution of the Peak-to-Average Power Ratio in OFDM Signals", IEEE transactions on communications, vol.49, no.2, February 2001.
- [4] Reddy, M.P., Rao, G.K., Kumar, D.H. et al. "Uplink coverage enhancements for extremely large-cell sites". J Wireless Com Network 2022, 57 (2022). <https://doi.org/10.1186/s13638-022-02133>
- [5] Khan, M., Rao, K., Amuru, S. et al. "Low PAPR reference signal transceiver design for 3GPP 5G NR uplink". J Wireless Com Network 2020, 182 (2020). <https://doi.org/10.1186/s13638-020-01787-1>
- [6] D. Boley and R. Maier, "SCFDMA Single Carrier FDMA in LTE", in Third SIAM Conference on Applied Linear Algebra, IXia Product Brochure , Nov.2009.
- [7] John G. Proakis "Book Chapter-6: Efficient Computation of DFT: Fast Fourier Transform Algorithms", 2018, pp. 448-498.



**Hari Krishna Boyapati** was born in Andhra Pradesh. He did his BTech in Electronics and Communications from RVR and JC College of engineering, Guntur and M.S by Research in Telecommunication Systems Engineering from IIT Kharagpur in 2012. Currently he is working as a Member Research Staff in Central Research Laboratory (CRL)- Bharat Electronics (BEL), Bangalore since 10 years. His research interests include physical layer development in ORAN based 5G Radio Units, long range-high data rate OFDM based radios, MIMO signal processing algorithms, and surface to air communication systems. He has 2 Indian patents and 15 publications in various IEEE and international conferences.



**Rajeev Kumar Elubudi** has received B.Tech in ECE from Andhra University in 2009 and M.Tech in Signal Processing and Communications from IIT Kanpur in 2011. Since 2011 he has been with Central Research laboratory, Bharat Electronics Ltd, Bangalore as Member (Senior Research Staff). His research interests include design and implementation of wireless communication systems.



**Shashikant Chaudhari** completed his M.E. in Electronics & Control from BITS Pilani in Dec 1997 & joined Central Research Laboratory (CRL) of Bharat Electronics Ltd (BEL) through Campus Selection in March 1998. From March 1998, he worked in projects such as nx32 E1 Digital Cross Connect and multiplexer for telecom segment. He worked on multimedia streaming and MPLS for joint projects with IISc Bangalore. Later, he was involved in the design and development of various Network Encryptors, Data Links, Radio on the move, Wi-Fi solution, LTE based solution for defence segment. Presently, he is working as Group Head for Wireless Networks Group of CRL BEL, concentrating on 5G base station solution, radio for Metro's rail communication, OFDM based radios, IRNSS/G3I based receivers and time servers etc. He is PMP certified.

# Custom Secure Remote Management Module for MCT Switch

Kunal Mohan Sadalkar  
 Member Senior Research Staff,  
 Crypto and Network Systems,  
 Email:sadalkarkunalmohan@bel.co.in

**Abstract**— Network element system provides various configurable and managerial parameters to tweak the default system's parameters. System designers always prefer to provide easy approach to the end user in order to manage device remotely over the IP network. There are various mechanisms evolved over the time by system designers to manage device remotely. These mechanisms developed as a service on the devices facilitating remote management feature. In this paper we will discuss, one of the mechanism called Secure Socket Shell (SSH) implemented and configured in MCT (Mobile Communication Terminal) L3 switch. The challenges faced to implement this module in custom ARM board and making it compatible with older Cisco devices. We followed secure development methodology to identify security requirement for BEL developed MCT L3 switch, implemented remote secure management feature and the challenges overcome to make it compatible with the COTS (Commercial Of The Shelf) router .

**Index Terms** --- *Secure Socket Shell, remote management, network security, authentication etc.*

## I. INTRODUCTION

Today, network element systems are used in a variety of broader industries such as telecommunication, logistics, space, healthcare, etc. They are designed and developed for dedicated functionalities to tackle specific problem in the industry. These systems are now capable of being connected over the internet using the "Internet of Things" for the improvement of manufacturing and distribution of goods and services, thanks to recent industry 4.0 evolutions. For the sake of speed and ease, these devices are accessed and managed remotely. However, the vast majority of these devices are vulnerable due to an insecure software stack or a default insecure configuration. Insecurity and vulnerabilities in these devices are exploited remotely by cyber criminals and converted these systems into bots for DDoS (distributed denial of service) attacks or to run as crypto-miners [1] [3]. Therefore, it is of the utmost necessity to secure these devices using a secure software development process (SDLC) and continuous security assessment.

Typically, network element devices have to perform three distinct activities:

- Process the transit traffic (Data Plane)
- Build common conscience with the surrounding network elements (Control Plane)
- Allow owner/user to configure, monitor and manage network element (Management Plane)

Control plane makes use of routing protocols such as OSPF (Open Shortest Path First), EIGRP (Enhanced Interior Gateway Routing Protocol), BGP (Boarder Gateway Protocol) etc. to discover adjacent devices and the overall network topology. Data plane that switches data from one interface to another and also referred as a forwarding plane. Interfaces, IP, routing protocols are configured using management protocols such as SNMP (Simple Network Management Protocol), HTTPS (Secure Hyper Text Protocol), SSH etc. Newer generation devices support RESTful protocols for managing devices remotely [4].

In most appliance-based network element solutions, the architecture consists of both hardware and software components. Figure 1.1 shows typical system architecture for network routing elements. Top layer is an application and services layer that interfaced directly with the user for configuring and managing its functional capabilities. The middle layer is an OS layer that takes care of scheduling, memory management, IPC (inter-process communication), etc. Below this hardware layer, which consists mainly of an SoC with NAND memory for running an OS (operating system) and a FPGA (Field Programmable Gateway Array) processor for packet forwarding. The capacity and performance is based on the underlying hardware architecture and the firmware running on top of the hardware.

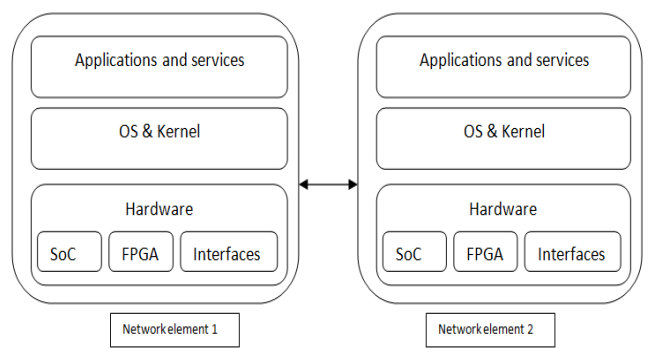


Figure 1: Block diagram of typical interconnected network devices

## II. REMOTE MANAGEMENT MECHANISMS

Networking devices are designed to manage locally as well as remotely. Local management requires physical adjacent to the device. However, remote management capability in the device enhances usability and accessibility from remote location. It

enables end user to access and configure device remotely without compelling to present physically. Over a period time remote management mechanisms have been evolved to suffice user requirements. Following section covers different techniques adapted by network devices along with pros and cons.

#### A. Telnet

Telnet (short for teletype network) is an oldest and more common mechanism supported by embedded devices due to its simplicity. It is client/server application protocol for virtual terminal service. Commonly it uses TCP port 23 and transfers data in clear text including user name and password. Because of this disadvantage, it is been avoided to use in network environment where security requirements are stringent.

#### B. Web Based:

As the services and features provided by network element increased over a period, traditional way of remote management such as telnet became obsolete. Moreover, increase in demand for better look and feel with management capability pushed to adapt web based remote management mechanism. It commonly uses HTTP/S service running on device which serves web based presentation layer (User Interface) to manage system effectively. The major disadvantage of web based management is slow method as compare to other mechanism.

#### C. Secure Shell:

One of the industry standard is to manage device remotely is secure socket shell (SSH). This is a cryptographic network protocol for operating network services securely over an unsecured network. It was designed on Unix like OS, as a replacement for more unsecure protocols such as remote shell, rlogin, rexec etc. which transfers data in clear text. Other than secure remote access, SSH provides plenty of network administration features such as tcp port forwarding, tunneling and X11 connection for GUI access. It also acts as base secure communication protocol for other application such as secure file transfer (SFTP) and secure copy between systems (SCP). SSH utility primarily comes default with the Linux/Unix systems installation. Historically, this utility has been evolved. Following is the brief description about chronological evolution of SSH as a service protocol.

#### SSH Version 1:

It was firstly developed in 1995 by a researcher at Helsinki University of Technology, Finland. The goal of this version was to overcome short comings of traditional remote login utilities which transfers data in clear text. It was estimated that by year 2000 the number of active users were 2 million. It consists of following three major protocols

- a. SSH-TRANS: It is the transport layer protocol basically used for server authentication, confidentiality and integrity.
- b. SSH-USERAUTH: It is used for user authentication at communication establishment. This authenticates SSH client to the SSH server.

- c. SSH-CONNECT: It multiplexes encrypted data into logical stream. This protocol runs on top of SSH-USERAUTH.

However, SSH-1 has serious structural weakness that leaves it vulnerable to broad number of attacks. These vulnerabilities have been addressed in SSH-2

#### SSH Version 2:

As the popularity of the utility grown multifold and many have adopted as de facto standard for secure remote management solution, in 2006 IETF working group came with the version 2 protocol standard called SSH-2. It has both security and feature improvement over SSH-1. Stricter security has been achieved by using wide range of key exchange protocol and the message integrity with message authentication check.

Version 1.99: After release of version 2.1, in RFC 4253, it is specified that all SSH server versions 2.0 and prior to it should identify it as 1.99

### III. MCT SWITCH ARCHITECTURE AND FEATURE

MCT (Mobile Communication Terminal) is a BEL made network switch designed and developed on Intel's Aria FPGA board along with ARM SoC running AngStrong embedded Linux for managing control plane. Following block diagram shows basic architecture of single card 8 port MCT switch.

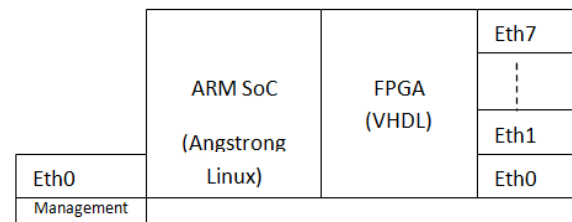


Figure 2: Basic Block diagram of MCT L3 switch

It makes use of community developed FRR (Free range routing) services for implementing routing protocols (Control plane). To manage, it makes use of different OS services, such as SSH, SNMP, AAA (Authentication Authorization and Accountability) etc. in the management plane. The MCT L3 switch can be configured using CLI (Command Line Interface) management terminal as well as web interface (GUI). Along with the other functional requirements, following security requirements are identified to make it secure.

- a. BGP authentication using MD5 (Message Digest) algorithm
- b. Password encryption for terminal services
- c. Custom SSH based secure remote terminal access
- d. Radius based authentication for switch
- e. Sticky MAC requirement for given 5 MAC addresses.
- f. Password Recovery mechanism

For the current development version except (f), all other security requirements are implemented successfully.

#### IV. PROBLEM SCOPE AND OBSERVATIONS

- a. MCT L3 switch makes use of default telnet based remote management mechanism. VAPT (Vulnerability Assessment & Penetration Testing) security audit report recommended that this telnet mechanism is unsecure protocol and transfers data in clear text.
- b. Hence, MCT L3 switch moved to more secure protocol called SSH for the remote management. Default SSH version configured in MCT L3 switch lacked key exchange algorithm support for older versions of SSH service.
- c. Therefore, MCT L3 switch not able to establish secure connection with the other COTS switches particularly SSH versions running with the older version.
- d. A SSH module has to be re-implemented by updating crypto libraries to make it backward compatible.
- e. Another observation is that all the SSH sub-module needs to be cross compiled for ARM architecture, unlike all the references on internet provided for X86 based architecture.

#### V. DESIGN AND IMPLEMENTATIONS

To realize secure remote management feature on MCT L3 switch, we made use of reference development from OpenSSH software version 8\_8 [5].

OpenSSH service makes use of OpenSSL library for the key exchange and encryption of data message. First, we observed that the default SSH service running on the underlying Arm board is missing the openssl library (libcrypto.so). Instead, it is bundled with the default system crypto library (libcrypt.so) package.

In first step, we downloaded open ssh package from authorized website [5]. We followed following steps to customize and cross-compile for arm architecture. It is assumed that all the pre-requisite for cross-compile has been configured on operating system. We used Ubuntu (Debian) OS as a base operating system for building SSH program.

##### A. Download & build zlib [8]:

It is designed to be general purpose lossless data -compression library virtually support for any computer hardware or software. Following commands are executed on ARM SoC to cross compile zlib package. Make command compiles binary and make install copies binary to \$HOME/zlibArm

```
CC=arm-linux-gnueabi-gcc
./configure --prefix=$HOME/zlibArm
make
make install
```

##### B. Download & build openssl [6]:

This is a secure socket library, and it is easy to find at the OpenSSL source code specifically do not need the "engine" variant, which uses hardware that does the heavy-duty crypto. Following commands cross compiles openssl library using make linux command. Before compiling environment variable "cross" is defined with "arm-linux-gnueabi-"

```
cd ./openssl-xxx
```

```
export cross=arm-linux-gnueabi-
make CC="$cross{gcc} AR=$cross{ar}
RANLIB="$cross{ranlib}"
make install
```

##### C. Download & build openssh [5]:

This is the SSH client & server itself. It is reference implementation for RFC4253. Following command configures openssh with all the pre-requisite libraries compiled in previous section b,c and builds openssh binary using "make" command.

```
./configure --host=arm-linux --with-libs --with-zlib=$HOME/zlibArm --with-ssl-dir=$HOME/opensslArm --disable-etc-default-login CC=gcc-arm-linux-gnueabi-gcc AR=gcc-arm-linux-gnueabi-ar && make
```

#### VI. TEST AND RESULTS

Following figure 3 shows the test-bed setup and different test cases covered to check functioning and compatibility with the COTS router. We have used Cisco router's COTS reference implementation for compatibility test. In test-bed Cisco old refers to model 2911 and Cisco new refers to model 8300 [5].

- a. SSH compatibility test from MCT (M) to Cisco New router (CN)
- b. SSH compatibility test from MCT (M) to Cisco old router (CO)
- c. SSH compatibility test from MCT (M) to MCT L3 switch (M)
- d. SSH compatibility test from Cisco New (CN) to MCT (M)
- e. SSH compatibility test from Cisco old (CO) to MCT (M)

Following table 1 shows the compatibility test result observed between MCT and Cisco router: In the below table, M is used for MCT L3 switch, CN is used for Cisco New and CO is for Cisco old. As we are testing protocol compatibility between MCT and Cisco old/new router, test cases among Cisco router are show as NA (Not Applicable). From and to describes start and end of SSH connection.

Table1: SSH protocol compatibility test between MCT L3 and COTS

From/To	M	CN	CO
M	✓	✓	✓
CN	✓	NA	NA
CO	✗	NA	NA

The above table depicts, the configured and implemented secure remote management service in MCT is compatible with

the COTS router configuration except the case cisco old to MCT. The compatibility test case failed due to the Cisco's old router uses SSH client with deprecated and vulnerable crypto algorithm [7].

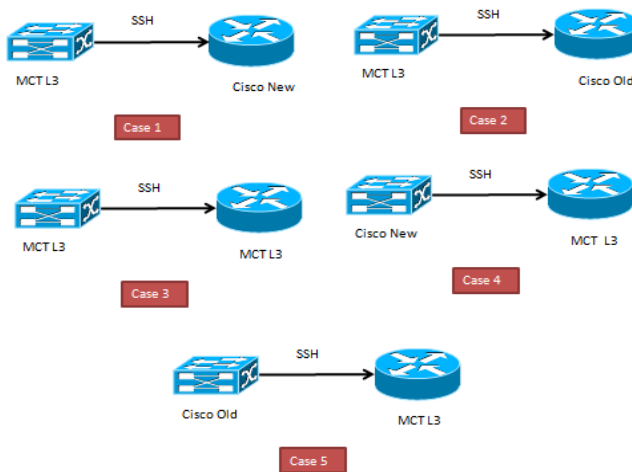


Figure 3: Test-bed setup for Protocol Compatibility Test between custom and COTS SSH



**Kunal Mohan Sadalkar** completed M.Tech from National Institute of Technology, Karnataka (NITK) in Informational Security in 2011. He is working as Member Senior Research Staff at Central Research Laboratory of Bharat Electronics Limited, Bangalore since August 2011. He has 12+ years of experience in cyber security domain as a developer and security auditor. He has presented papers in information security domains in national and international conferences. He has lead the team for CERT-in empanelment for VAPT and obtained certification.

Areas of interest include software and embedded security, VAPT methodology, malware analysis, SIEM, network protocol security, cryptanalysis, cyber-warfare and offensive technologies

## VII. CONCLUSION

For automation and configuration, almost all network embedded systems and network devices today require remote management. Many system designers take the path of implementing unsecure protocols such as telnet, rlogin, etc. These remote access management methods do not pose a major threat when used in a closed, trusted network system, but as these devices are connected to a larger internet system, the threat effect multiplies. Therefore, these devices need to be accessed with the secure management protocol for remote terminal access. In this paper, we identified requirement and need for secure remote management for network devices. The challenges faced in implementing secure remote management for ARM based custom MCT L3 switch board and the protocol incompatibility issue between MCT and COTS router. Finally, the customized SSH service utility is implemented with resolution of the compatibility problem and makes MCT L3 switch secure for remote access.

## REFERENCES

- [1] Vitor Pedreira, Daniel Barros, Pedro Pinto, "A Review of Attacks, Vulnerabilities, and Defenses in Industry 4.0 with New Challenges on Data Sovereignty Ahead", *Sensors*, vol.21, no.15, pp.5189, 2021
- [2] M. M. Raikar and S. M. Meena, "SSH brute force attack mitigation in Internet of Things (IoT) network : An edge device security measure," 2021 2nd International Conference on Secure Cyber Computing and Communications (ICSCCC), Jalandhar, India, 2021, pp. 72-77, doi: 10.1109/ICSCCC51823.2021.9478131.
- [3] <https://www.csk.gov.in/alerts/mirai.html>.
- [4] <https://blog.ipspace.net/2013/08/management-control-and-data-planes-in.html>.
- [5] <https://www.openssh.com/>
- [6] <https://www.openssl.org/>
- [7] <https://techblog.cisco.com/>
- [8] <https://zlib.net/>.

# Establishment of Private Wireless Network Using Open-source Software Magma

Soubhik Baral  
Central Research Laboratory  
Bharat Electronics Ltd.  
Bangalore, India  
soubhikbaral@bel.co.in

Chaitanya P. Umbare  
Central Research Laboratory  
Bharat Electronics Ltd.  
Bangalore, India  
umbarechaitanya@bel.co.in

Jeevitha L  
Central Research Laboratory  
Bharat Electronics Ltd.  
Bangalore, India  
jeevithal@bel.co.in

Nidhi Jain  
Central Research Laboratory  
Bharat Electronics Ltd.  
Bangalore, India  
nidhijain@bel.co.in

**Abstract**—In order to address the challenges of rural internet access, open source software Magma provides a flexible low-cost and scalable network solution. Magma ensures minimal development and deployment effort with access network agnostic. Evolved packet core is a vital component of a cellular network to provide any communication services or internet. This open source software Magma is a next-generation packet core that supports 4G LTE or 5G radios or any wireless network. This paper presents the establishment of private network on Citizens Broadband Radio Service band (CBRS: 3550Mhz to 3700Mhz) over 4G LTE network using Magma software deployed in KU551 kit. This private network deployment comprises Baicells Atom ID06G Customer Premise Equipment (CPE) for each client, Baicells Neutrino 430 eNB for 4G base station, i-7 processor based kit (KU551) for Magma Core Network (CN) and a server connected with KU551 for SIP communication.

**Index Terms**—Private Network, Magma, CBRS, CPE

## I. INTRODUCTION

Establishment of Private Network in any organization enhances adaptability, security and effectiveness. With the establishment of Private Network, enterprises can have control and choice to make modifications on the network based on their requirements like reach of a network, quick network failure recoveries, maximum limit of a network and more [1].

Wi-Fi being the popular solutions for Private Network has some drawbacks. Wi-Fi doesn't uphold huge Internet of Things (IoT) administrations because of the restricted association per channel, Wi-Fi also has security concerns which is not favourable for any defence organizations [2]. Table I list the differences between Wi-Fi 6 and Private 5G. Wi-Fi also have restricted facilities when it comes to new technologies like self-driven car, smart cities etc. In contrast to that, Private 4G/5G networks can meet all such advance needs in recent times and also in near future [2].

With advancement of technologies in telecommunications, many companies need secure, reliable and fast private network which covers large areas and allows secure voice and data communications in the organization. Some enterprises also depends on Private Network environment for carry their

TABLE I  
DIFFERENCES BETWEEN WI-FI 6 AND PRIVATE 5G

	Spectrum	Security	Reliability	Coverage
Wi-Fi 6	Low	Low	Low	Low
Private 5G	High	High	High	High

experiment and research need. Hence, open-source platforms can fulfil such requirements [3].

Private Networks can be established with the help of licensed mobile network operator but it is an expensive solution. Magma is an open-source software platform which enables network operators a flexible, open and extendable mobile core network. This paper presents the building of 4G enterprise grade private mobile network using unlicensed CBRS band. This Magma open source software is implemented on KU551 kit. We have also implemented Magma on SMARC Conga SA5 and I-Pi SMARC plus but due to poor performance we decided to use KU551 kit. This network setup comprises Baicells Atom ID06G CPE for client and Baicells Neutrino 430 eNB for 4G LTE base station. Baicells Atom ID06G CPE, Baicells Neutrino 430 eNB was used as it supports CBRS band which can be used to establish private network for our requirement.

After establishment of Private 4G LTE network, the following test-cases were also verified:

- 1) Attachment of Base station (eNodeB/gNodeB) to the Magma Core Network.
- 2) CPE's (2) attachment to Base Station and Magma Core Network (CN).
- 3) Uplink/Downlink throughput for TCP/UDP traffic.
- 4) Voice call between two CPE's over SIP

The paper contents are divided into 2. Literature Review 3. Methodology provides in-depth details on how Magma and Baicells Indoor eNodeB-pBS31010 is used for the set up private network 4. Test Results and finally we conclude with 5. Conclusion and Future work.

## II. LITERATURE REVIEW

Like never before, Private Network is in huge demands with the advancement of AI technologies like robots ,self driving car,drones,sensors etc.Private Networks provides services to those devices that requires scalability, security, availability. Private Networks will assist with working on the worth of the venture by giving foundation that can keep on developing [2].

Additionally, in this present reality where information breaks are quite common, high-innovation modern organizations require the utilization of their own modified security strategies and privately put away information, which may not be upheld by a portion of the customary public cell organizations. Because of these deficiencies, private organizations, which are likewise named non-public organizations in the third Generation Partnership Project (3GPP) [4], have drawn in huge interest.

Magma open-source platform has evolved as a community, and with major collaborations it provides its community to build advance networks [5] which supports Wi-Fi,LTE,5G communications. It can deftly uphold a radio access network with negligible turn of events and arrangement exertion, and incorporates three significant parts:Access Gateway,Orchestrator,Federation Gateway.

## III. METHODOLOGY

With the increase of business requirement of private 4G/5G network, Magma the open-source Mobile core solutions provides cost-effective, reliable, scalable and feasible solutions for operators providing network accessibility in remote areas. Fig 1. depicts the high level Magma architecture which is 3GPP generation and access network agnostic. The key components of Magma architecture are Access Gateway (AGW), Orchestrator (ORC8r) and Federation Gateway (FEG). A typical Magma network will have many AGW for scaling with radio network. In Magma, the Access Gateway provides the network services and policy enforcement. The AGW is light weight software that provides EPC (Evolved packet core) functionalities and it contains MME (Mobility Management Entity), S-GW (Serving Gateway), P-GW (Packet Data Network Gateway) as some of the components. The major functionalities of AGW is subscriber registration, authorization, subscribers mutual authentication, IP address allocation to subscriber, subscriber deregistration, upgrading current serving MME id of the subscriber to HSS, pull the subscriber data from HSS, tracking of inactive subscribers etc. The orchestrator plays vital role in setting up a network and it allows configuring and monitoring the entire network and gateways centrally. The Network Management System (NMS) of Orchestrator is based on REST API that allows configuring AGW such as adding subscriber and policies to the network and displays the current status of network. Orchestrator is built with micro services frame work and it can be deployed in public or private cloud. The micro services of orchestrator are nghttpx, obsidian, certifier, bootstrapper, config, streamer, metricsd and datastore. The Federation Gateway is an optional component which acts

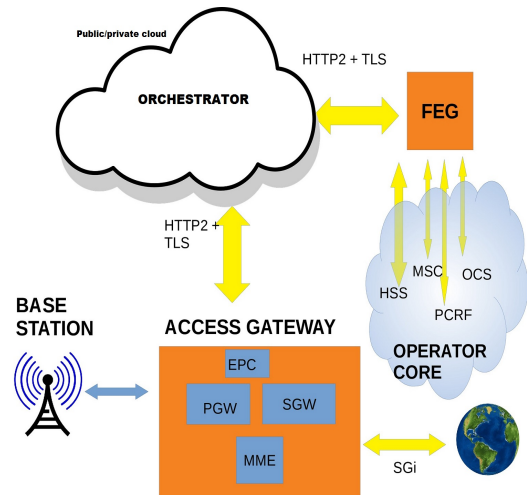


Fig. 1. Magma Architecture

as a proxy between Magma AGW and operator's network and facilitates major functions such as policy enforcement, data plans, authentication and charging to stay uniform between an existing MNO networks. This federation gateway expands the Magma with operator's network. Without federating onto and existing mobile core Magma can operate in stand-alone mode. This paper presents a 4G LTE private network without Federation gateway. The Fig 2. depicts the overall workflow of our 4G LTE private establishment. The main components in this setup are Magma, Baicells Indoor CPE and Baicells Indoor eNodeB. Magma was deployed on i-7 processor based kit (KU551) which Provides important framework like MME, HSS, SGW, PGW for providing data and voice LTE services. The Baicells Indoor eNodeB base station connects devices like mobile phones/ CPEs to core network using CBRS radio frequency is configured. Magma uses eth1 as the default S1 interface. Hence to connect our eNodeB to the Magma gateway eth1 interface was used. Magma's enodebd service can also be used for automatic eNodeB connection but here we have configured manually. After successful attachment of eNodeB and Magma EPC, Magma will be running a DHCP server to assign an IP address to the connected eNodeB, which gets IP 192.168.60.245 from the Magma core network. The assigned IP address to the eNodeB can be verified using the dnsd service. To check for successful attachment of eNodeB and core network s1 traffic was validated. Now CPE's can be attached to the network once when eNodeB starts transmitting. CPE's attachment can be success- ful once AGW accepts the authentication based on configuration of IMSI, APN and other network configuration. For CPE's attachment, network configuration such as APN, subscriber needed to be configured under Magma's APN. Once the Magma's AGW picks the APN configuration CPE1 and CPE2 are connected to the Network. Both the CPEs were allocated IPs, under APN by the Magma Access Gateway, the IP range can be set in the NMS. The

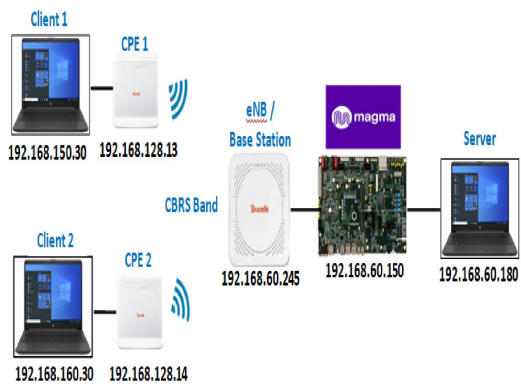


Fig. 2. 4G LTE private network setup

server in the network is used to check the uplink and downlink traffic of client1 and client2 which are connected to the CPE1 and CPE2 respectively. Server is also used as a SIP proxy for making voice calls between client1 and client2.

The Network Management System (NMS) of the Magma orchestrator is used for the core network functionality and GUI provided by Baicell's for CPE is used for its configuration.

Overall software/hardware platforms used for End to End private 4G/5G Test Bed setup:

- 1) Magma Core Network (CN)
- 2) Baicells Indoor eNodeB
- 3) Baicells Indoor CPE
- 4) Client 1 for CPE1
- 5) Client 2 for CPE2
- 6) Server

#### A.Magma Deployment

The aim of Magma was to provide mobile core solutions that are cost-effective, reliable, scalable and accessibility in remote areas. Magma followed the basic principle of SDN that is separation of control plane from data plane. Access Gateway stores the run-time states at the edges, whereas Orchestrator stores the configuration states which allow UE's like mobile phones to connect to the network. The EPC functionalities are configured in Magma's Access Gateway (AGW) which relays the run-time functionality to the Orchestrator. Magma Access Gateway (AGW) is deployed on Ubuntu 20.04 and also can be deployed using Vagrant and VirtualBox [9]. For the deployment of AGW, hardware configuration required are shown in TABLE II. Vagrant is an open-source software product for building and maintaining portable virtual software development environments. We have deployed AGW using Vagrant and VirtualBox on i-7 processor based kit (KU551). Following every step for deployment of Access Gateway using Vagrant and VirtualBox in Ubuntu 18.04 as per reference [9] we have installed our Magma Mobile core.

TABLE II  
HARDWARE CONFIGURATION FOR DEPLOYMENT OF ACCESS GATEWAY

FACET	VALUES
Magma Tag	v1.6
OS	Ubuntu 18.04
vCPU	4
RAM	(16 GB)
Memory	(90 GB)

TABLE III  
AGW AND ORCHESTRATOR IP'S FOR TEST BED SETUP

FACET	VALUES
Magma Tag	v1.6
AGW IP	192.168.60.150
AGW OS	Ubuntu 18.04
Controller IP	192.168.60.248
Bootstrapper IP	192.168.60.248
Fluentd IP	192.168.60.247

The Orchestrator functionality can be implemented in private or a public cloud. Here we have deployed Orchestrator using Docker and have registered it in Docker hub account using scripts provided in Magma repository.

By accepting the self-assigned certificate provided by the Magma [10] we used NMS for controlling and Management of the Network. NMS was used to configure our gateways and related eNodeBs. After proper deployment of AGW and Orchestrator, using the NMS, configuration was made for AGW connection. TABLE III shows the characteristics for Orchestrator and AGW.

#### B.Baicells Indoor eNodeB

The Baicells Neutrino430 is a high level two-transporter indoor eNodeB (eNB) consistent with 3GPP LTE TDD innovation. Baicells Indoor eNodeB works on Carrier Aggregation (CA) mode or Dual Carrier (DC)/split mode. It supports HaloB operating mode which is necessary to core network functions of the eNB. Fig. 3 depicts the basic eNodeB settings that are configured for our network. Fig.3 shows the Basic configuration information of eNB.

After connection of AGW with the Orchestrator, we provisioned our eNodeB in NMS. We have manually configured eNodeB by enabling the "eNodeB managed externally" option under RAN settings. To add subscribers to the network, we initially provisioned an Access Point Network. APN can be easily added using the "ADD APN" functionality under APN configuration in NMS. After adding APN any number of UEs/CPEs can be attached to the network. Here we have added two CPEs for testing our network.

#### C.Baicells Indoor CPE

Customer Premise(s) Equipment, which points to any connected equipment that is basically used for accessing web or getting the services from the service providers whether connected directly to the network or indirectly connected to the network. Baicells CPE provides wireless access and routing functionalities to bring data and voice services to end-users. It transforms high speed Long-Term Evolution (LTE) Time

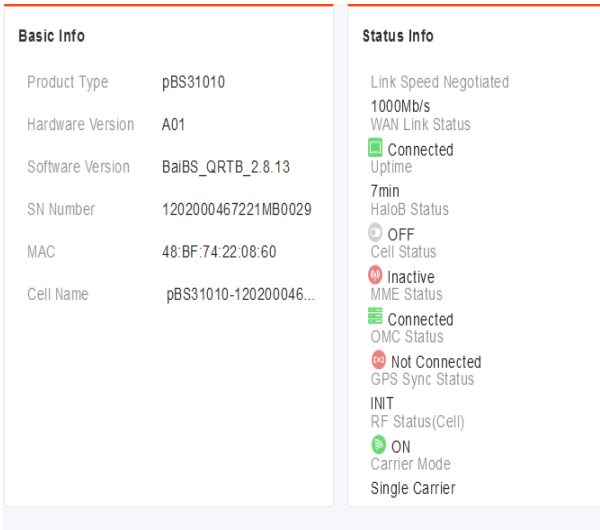


Fig. 3. eNodeB Settings

Division Duplexing (TDD) signals over CBRS band on the local area network (LAN).

After adding the APN as mentioned in the previous section, CPEs needed to be attached to the network. CPE can be configured either by Baicells Indoor CPE's GUI locally or remote web management of Magma core network. Fig 4 shows the GUI-based management portal that is used for our network configuration.

After the configuration of CPEs, AGW picks the APN for CPE1 and CPE, and are connected to the network. Once after the successful attachment of the CPE to the network both the CPEs were assigned IPs, under APN configuration provided by the Magma. In this established 4G LTE private network over CBRS band, SIP voice call communication is tested between client1 and client2 with SIP proxy server.

#### D.Client 1 and Client 2

Client1 is connected to CPE 1 and client2 is connected to CPE 2 over LAN. To establish voice communication VOIP clients are installed on client1 and client2. User ID for client1 and client2 was set as 9001 and 9002 respectively. Clients are also used to access the GUI of CPEs for the configurations of network. Some examples of VOIP Clients are Blink Call, Ekiga, Jitsi etc.

#### E.Server

Server was installed behind the magma for the checking of Uplink and Downlink traffic to and from the Server. Here we have verified both TCP and UDP traffic flow. For VOIP communication we have set your own VoIP server. Asterisk server was installed as a VOIP server. To make communication with our VOIP clients we have registered 2 users 9001 and 9002 under SIP.conf file in Asterisk.

## IV. TEST RESULTS

In this section we come up with the results for the test-case mentioned above:

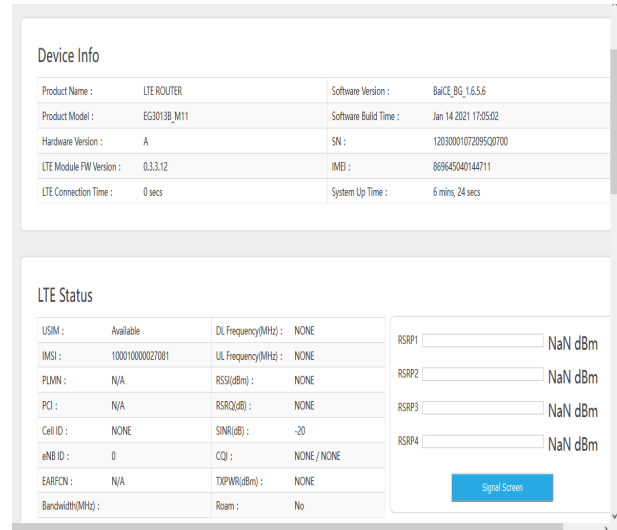


Fig. 4. CPE's GUI based device information

Source	Destination	Protocol	Len Info
192.168.60.147	192.168.60.150	S1AP/NAS-E..	218 InitialUEMessage, Attach request, PDN connectiv..
192.168.60.150	192.168.60.147	S1AP	102 UEContextReleaseCommand [NAS-cause-detach]
192.168.60.150	192.168.60.147	S1AP/NAS-E..	94 DownlinkNASTransport, Identity request
192.168.60.147	192.168.60.150	S1AP/NAS-E..	146 UplinkNASTransport, Identity response
192.168.60.150	192.168.60.147	S1AP/NAS-E..	142 DownlinkNASTransport, Authentication request
192.168.60.147	192.168.60.150	S1AP	102 UEContextReleaseComplete
192.168.60.147	192.168.60.150	S1AP/NAS-E..	138 UplinkNASTransport, Authentication response
192.168.60.150	192.168.60.147	S1AP/NAS-E..	122 DownlinkNASTransport, Security mode command
192.168.60.147	192.168.60.150	S1AP/NAS-E..	146 UplinkNASTransport, Security mode complete
192.168.60.150	192.168.60.147	S1AP/NAS-E..	114 DownlinkNASTransport, ESM information request
192.168.60.147	192.168.60.150	S1AP/NAS-E..	146 UplinkNASTransport, ESM information response
192.168.60.150	192.168.60.147	S1AP/NAS-E..	282 InitialContextSetupRequest, Attach accept, Activ..
192.168.60.147	192.168.60.150	S1AP	12.. UECapabilityInfoIndication, UECapabilityInformat..
192.168.60.147	192.168.60.150	S1AP/NAS-E..	182 InitialContextSetupResponse, UplinkNASTransport,
192.168.60.150	192.168.60.147	S1AP/NAS-E..	134 DownlinkNASTransport, EMM information
192.168.60.147	192.168.60.150	S1AP	86 UEContextReleaseComplete

Fig. 5. CPE attached to Base Station and Core Network

- 1) **Attachment of Base station (Baicells Neutrino 430 eNodeB) to the Magma Core Network:** Fig 6. shows S1SetupRequest and S1SetupResponse which validates the attachment of base station with eNodeB. Fig 7. shows that over GUI of eNB that MME is connected to the Base Station which also validates the Attachment of Base Station to the Magma Core Network.
- 2) **Attachment of CPE ( Baicells Atom ID06G)** Fig 5. shows that requested CPE attachment was successfully granted by eNB and Core Network (CN).
- 3) Verified Uplink and Downlink throughput for TCP/UDP traffic and also voice call between the CPEs using SIP proxy

## V. CONCLUSIONS AND FUTURE WORK

This Paper presented the private network establishment based on 4G LTE over CBRS band, the network setup comprises Baicells indoor eNodeB Base station, Baicells indoor

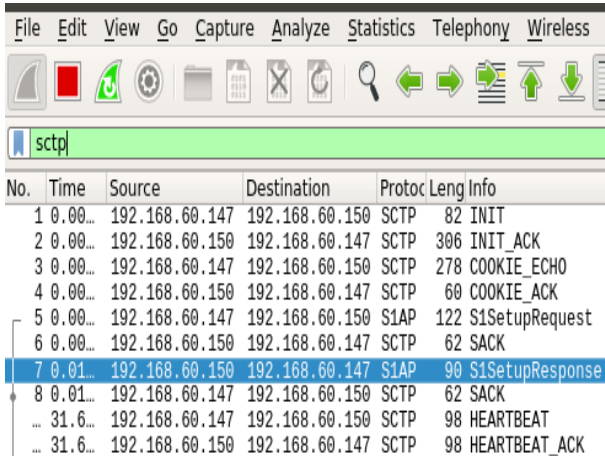


Fig. 6. Magma(CN) and Baicells Indoor eNodeB attachment.



Fig. 7. Magma(CN) and Baicells Indoor eNodeB attachment

CPEs for Client1 and Client2, KU551 kit for Magma deployment and server. This setup can be extended for the evaluation of 5G Standalone Mode (SA) using gNodeB. Further this work can be extended to integrate Federation Gateway (FEG) to scale up this private network with existing Mobile Network Operator(MNO). Here we have tested our network with one base station and 2 CPEs, which can be further scaled up to three base stations for wider range and multiple CPEs for checking the scalability of subscribers in the network.

## VI. ACKNOWLEDGEMENT

We thank our organization Central Research Lab of Bharat Electronics Ltd, Bangalore for providing support and required resources in order to carry out this work efficiently. Also, we would like to thank our colleagues for their insights on reviewing this work periodically and providing support during the development.

## REFERENCES

- [1] R. Ferrus and O. Sallent, "Extending the LTE/LTE-A business case: Mission- and business-critical mobile broadband communications", IEEE Veh. Technol. Mag., vol. 9, no. 3, pp. 47-55, Sep. 2014.

- [2] G. Brown, "Private 5G mobile networks for industrial IoT" in, Qualcomm Inc, 2019.
- [3] J. Liao and X. Ou, "5G military application scenarios and private network architectures", Proc. IEEE Int. Conf. Adv. Elect. Eng. Comput. Appl., pp. 726-732, 2020.
- [4] "Technical specification group services and system Aspects Study on management aspects of non-public networks (release 17)", 3GPP, no. TR28.807, Oct. 2020.
- [5] Navid Nikaein, Mahesh K. Marina, Saravana Manickam, Alex Dawson, Raymond Knopp and Christian Bonnet,"OpenAirInterface: A Flexible Platform for 5G Research", ACM SIGCOMM Computer Communication ReviewVolume 44,October 2014.
- [6] Navid Nikaein, Raymond Knopp, Florian Kaltenberger, Lionel Gauthier, Christian Bonnet, Dominique Nussbaum, Riadh Ghaddab"Demo: OpenAirInterface: an open LTE network in a PC" MobiCom '14: Proceedings of the 20th annual international conference on Mobile computing and networking, September 2014.
- [7] Ettus Research,The USRP Hardware Driver Repository, <https://github.com/EttusResearch/uhd>.
- [8] Openairinterface 5G Wireless Implementation,
- [9] Juan C. Caviedes V, <https://github.com/caprivism/virtualization/wiki/AGW-Deployment-using-Vagrant>.
- [10] Magma.<https://docs.magmacore.org/docs/basics/introduction.html>.



# 1. SWIR imaging module for ADEOS-LR

Karthick D  
Member (Research Staff)  
EOP, CRL  
Email: karthickd@bel.co.in

ADEOS-LR (Advanced Electro Optic System – Long Range) is a day and night surveillance system for observing targets up to a range of 20km. The system is capable of streaming live video on wired/wireless/optical link. The system primarily consists of a TI (Thermal Imager) and SWIR (Short-Wave InfraRed)channels. SWIR modulehosts a state-of-the-art real-time SWIR detector, continuous zoom optics and signal processing engine. Image processing algorithms are developed and incorporated to provide observation capabilities in day light, twilight conditions as well as under degraded visibility conditions. System functionality has been successfully demonstrated to Indian Army.

Table 1: Specifications of SWIR module

	Specifications		
Spectral band	0.9-1.5 $\mu\text{m}$		
Sensor type	InGaAs		
Active pixels	640(H)x512(V)		
Field of view	<ul style="list-style-type: none"> <li>• Wide <math>\geq 12^\circ \times 10^\circ</math></li> <li>• Narrow <math>\leq 0.8^\circ \times 0.6^\circ</math></li> </ul>		
Optical magnification	19x continuous		
Digital zoom	4x		
Modes of operation	Standard imaging (low gain), Low noise imaging (high gain)		
Algorithms	Multiple NUC tables (up to 9), Multi frameNUC, automatic integration time selection, DRC, Detail enhancement, bilinear interpolation, etc.		
Range		Human	Vehicle
	Detection	$\geq 15\text{km}$	$\geq 20\text{km}$
	Recognition	$\geq 08\text{km}$	$\geq 15\text{km}$
Physical dimensions	$\leq 650 \times 300 \times 300 \text{ mm}$		
Weight	$\leq 25 \text{ Kg}$		

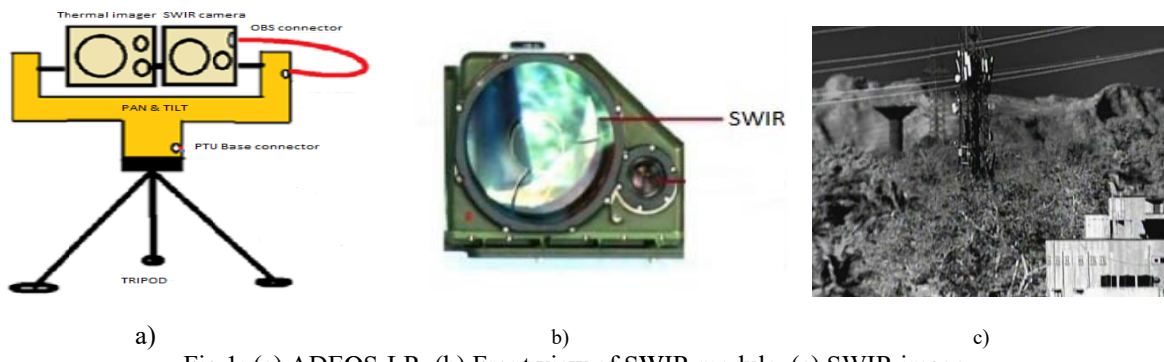


Fig 1: (a) ADEOS-LR, (b) Front view of SWIR module, (c) SWIR image

## 2. CPS MK II system for MBT Arjun

Nerella Arun Mani Kumar, Varanasi Krishna Priya

Member (Research Staff)

EOL&EW, CRL

Email:nerellaarunmanikumar@bel.co.in, vkpriya@bel.co.in

Commander Panoramic Sight (CPS) for MBT Arjun Mk I consists of Thermal Imager, LRF, Day Camera. In addition, it has interfaces for Fire Control Computer and Gunner's Main Sight. Thermal Imager in CPS MK II incorporates a state of the art SXGA (Super Extended Graphics Array) detector with  $10\mu\text{m}$  pixel pitch, a 19-275mm zoom lens and Signal Processing Board (SPB) and has a capability of observing targets more than 10km. Detector Non-Uniformity Correction (NUC), Defective Pixel replacement, and Image Processing algorithms for contrast enhancement, Sharpness control and Dynamic Range Compression(DRC) are incorporated in SPB to provide detection capabilities in Day and Night conditions. Integrated System functionality has been successfully demonstrated to CVRDE, Chennai at Pokhran field ranges.

Table 1: Specifications of CPS MK II module

Specifications	
Spectral band	3-5 $\mu\text{m}$
Sensor type	InSb (Black Bird 1280)
Active pixels	1280(H)x1024(V)
Field of view	<ul style="list-style-type: none"> <li>• Wide <math>\geq 15^\circ \times 11^\circ</math></li> <li>• Narrow <math>\leq 2.5^\circ \times 2.0^\circ</math></li> </ul>
Zoom Lens	15-275mm
Digital zoom	4x
Modes of operation	Standard imaging , Binning imaging (reduced spatial noise)
Algorithms	Multiple NUC tables (up to 3), Multi frame FNUC, automatic gain control (AGC), DRC, Detail enhancement, EZoom etc.
Ranges	MBT Arjun Tank (3.8m (W) $\times$ 2.3m (H))
	Detection $\geq 8\text{km}$
	Recognition $\geq 4\text{km}$



Fig 1: (a) Front view of CPS System, (b) CPS image

### 3. High Assurance Crypto System for Public Network

Jeevitha L, John Krishna Yaragorla, Hyndavi Rapuru, RamaRao Ramisetty, Nidhi  
 Jain Contact ID : jeevithal@bel.co.in

#### SYSTEM ARCHITECTURE

High Assurance Crypto System is an alternative technology to provide secure end to end system communication over public network. High Assurance crypto system comprises a system (PC) with software solution and multi channel Router which provides internet connection to the system (PC). This Multi channel Router supports 2 SIM card interfaces, 2 Ethernet interfaces and 1 USB interface for WAN (Wide Area Network) and 2 Ethernet interfaces for LAN (Local Area Network) connection. This multi channel router is configured with polices to send the data over selected WAN channel. The High Assurance Crypto System receives the File/ Mail data from its server and splits this data into random number of parts with random size and each part is encrypted by selecting encryption algorithm randomly from the encryption algorithm sets. Each encrypted data part is sent to the remote system by selecting randomly a source WAN channel of the local Router and destination WAN channel of remote Router and even few parts can be transmitted over relay systems. If the remote WAN channel contains Dynamic Public IP address then the corresponding encrypted data is sent to the service that runs on cloud environment and upon the successful authentication of remote system, receives its encrypted data from the service over the dynamic IP address based WAN channel. All these encrypted parts are transmitted over TLS (Transport Layer Security) protocol. Remote High Assurance Crypto System receives all the encrypted data parts and decrypts with its corresponding encryption algorithm. All these decrypted parts are merged and its integrity value is verified to obtain the original File/Mail data and then forwarded to its corresponding server.

The Fig.1 depicts the communication between three servers using High Assurance Crypto Systems over Public Network.

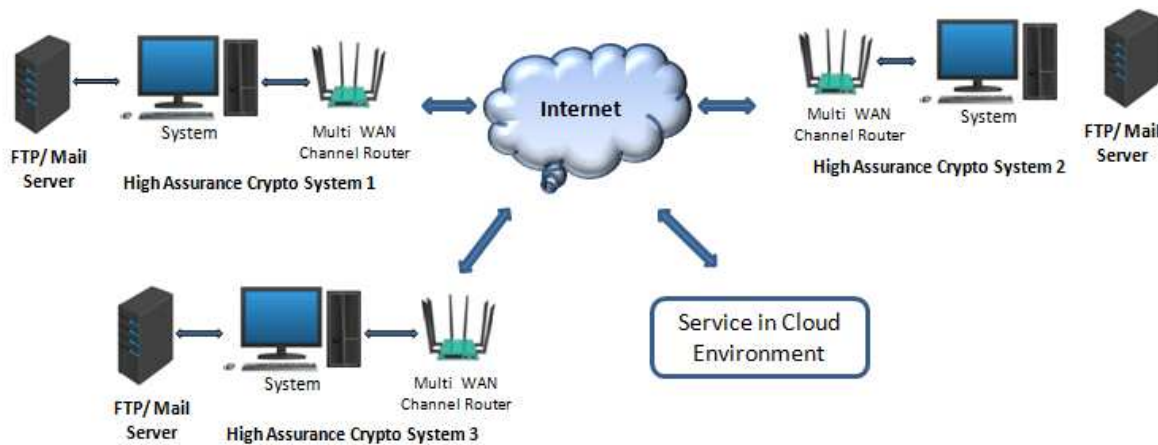


Fig.1 Deployment architecture

#### SALIENT FEATURES

- Establishment of secure scalable private network over Internet domain
- Secure transmission of File/ Mail application data over multiple wired and wireless WAN
- Multi level encryption
- Application data split by random number of parts with random size at source
- Random selection of encryption algorithm for each data part
- Random selection of source WAN channel and destination WAN channel for each encrypted part transmission and reception
- Encrypted parts transmission and reception over TLS protocol
- Relaying of data parts to introduce more obfuscation
- Integrity computation at transmission and its verification at destination system



## **Granded Patents**

1. Patent No. 429375

Date of Grant: 19.04.2023

Application No. 201941013402

Inventors: Nidhal M Mansoor (PDIC)

Rohan Jacob (PDIC)

Gaurav Lakhera (PDIC)

Meenakshi Ghai (CRL)

Putta Venkatesh (CRL)

**Title of Invention:** Systems and Methods for Providing Seamless Communications and Voice Quality Enhancement of VOIP

**Abstract:** A method for providing seamless service and voice quality enhancement for voice over internet protocol is provided. The method including duplicating (301) one or more packets for creating copies of the packets by a source node based on one of number of network connections between the source node and destination node and maximum number of copies of packets allowed in a single network. The copies are configured based on network parameters and are transmitted by the source node to the destination node. The destination node receives the packet and extracts an identifier from the received packet. The identifier is compared with the elements of a buffer. If the identifier exists in the buffer, that indicates the current packet is a duplicate, then the packet is discarded, else the packet, that is unique, is provided to a call manager or a packet switching engine and the identifier is stored in the buffer.

2. Patent No. 429408

Date of Grant: 19.04.2023

Application No. 201941013134

Inventors: Thejna Ros Joseph (CRL)

Lunavath Mahesh (CRL)

Renuka Sehgal CoE (EO & L)

Ranu Tyagi (CRL)

**Title of Invention:** A Method for Spectral and Temporal Measurements for Fiber Ring Laser

**Abstract:** The present invention is related to a measurement setup for measuring the spectral and temporal dynamics of a fiber ring laser is provided. The fiber ring laser includes a 2x2 fiber fused coupler (104) which couples out the optical power in a defined coupling ratio. Further, to monitor the spectral and temporal stability of the laser system, an unused input port of the fiber coupler is used. The 2x2 fiber fused coupler (104) includes a first and a second input ports (201, 202) and a first and a second output ports (203, 204). Further, the input signal light in the first input port (201) leaks out to the second input port (202), which is an unused port, due to back reflections inside the tapered fused coupled region in the 2x2 fiber fused coupler (104). The leaked signal light to the second input port (202) carries the signal light and monitors the spectral and temporal dynamics of the fiber ring laser.

## **Granded Patents**

**3.** Patent No. 410219

Date of Grant: 28/10/2022

Application No. 201941013402

Inventors: Shaik Abdul Subhan CoE (R & WS)

Nagendra Kumar Mangali (CRL)

Damodar Vishwanath Kadaba (CRL)

**Title of Invention:** Device and Method for Improved Mode Decoding in Transponder System.

**Abstract :**A device for decoding signals in transponder system, the device includes: at least one antenna for receiving one or more signals from a base station; at least one receiver assembly operatively coupled with the at least one antenna, said at least one receiver assembly configured to amplify the received one or more signals with enhanced selectivity; analog to digital converter (ADC) configured to receive the amplified one or more signals, and convert the amplified one or more signals to digital one or more signals at a predefined sampling frequency; a correlation unit configured to receive the converted one or more signals, wherein the converted one or more signals are pulse width matched with a pre-stored one or more sample signals stored in a first database, and generate a correlated one or more signals; a threshold unit configured to receive the correlated one or more signals and determine one or more threshold values based on changes in amplitude of the corelated one or more signals; a pulse detector unit configured to receive the one or more threshold values and the one or more corelated data and based on the received one or more threshold values determine one or more leading and the trailing edges of the one or more corelated; and a mode determination unit configured to receive the correlated one or more signals and the determined one or more leading and trailing edges, wherein the mode extractor unit configured to determine mode of communication based on the determined one or more threshold values, and the one or more leading and trailing edges.

**4.** Patent No. **410265**

Date of Grant: 04/11/2022

Application No: 201841036940

Inventors: Fahad Abdul Basheer Majida (CRL)

Gogulamudi Sampath Kumar CoE (R & WS)

Viji Paul Panakkal (CRL)

**Title of Invention:** A Method for Radar Bias Computation

**Abstract:** The present invention describes a method to compute the radar biases in range, azimuth and elevation using the GPS measurements. Further, the method effectively computes the bias in 3D radar without the need of multiple radars and thereby reducing the communication needs and computational complexity. This present invention is used for three dimensional surveillance radar tracking having measurements as range, azimuth and elevation. Further, this present invention automatically estimates radar biases timely based and propagates to the end user there by reducing the overhead head cost of measuring the biases.

## ***Granted Patents***

5. Patent No. **406259**

Grant Date: 09/09/2022

Application No: 201841036586

Inventors: Yellampallae Venkata Subba Rao (CRL)

Nidhi Jain (CRL)

**Title of Invention:** A Method to Determine Cyclic Redundancy Check for a Multi Frame Data Word

Abstract: The present disclosure provides a method for calculating cyclic redundancy check (CRC) for multi frame data words in a single clock cycle, especially for error detection in Ethernet applications. The input wide data word is split into 512 bit sub words. A number of combined intermediate CRC generation modules generate an intermediate CRC for each of the 512 bit sub words. The intermediate CRCs are combined with XOR logic combiner and inverted to derive final CRCs. In this method, the intermediate CRC generation modules shift the data sub words and perform XOR operations according to the frame endings occur in the input wide data word. This helps to calculate CRC in parallel for frames spread across multiple data sub words.



## ***Important Events at CRL***



***Visit of School of Artillery staff members on March 14, 2023***



***Republic Day Celebration on January 26, 2023***

## *Important Events at CRL*



**Republic Day Celebration on January 26, 2023**



**Techno Crunch Session on January 05, 2023**

## *Important Events at CRL*



***Visit of Principal Director Commercial Audit on January 12, 2023***



***Fire Safety Mock Drill on January 05, 2023***

## **Important Events at CRL**



**World Hindi Day Celebration on January 11, 2023**

# LIST OF UPCOMING CONFERENCES

1. IEEE Global Communications Conference  
4–8 December 2023 // Kuala Lumpur, Malaysia  
**IMPORTANT DATES**  
Workshop Paper Submission Deadline: 15 July 2023  
Acceptance Notification: 1 August 2023  
Camera-Ready Submissions: 1 September 2023
2. IEEE International Conference on Communications  
9–13 June 2024 // Denver, CO, USA  
**IMPORTANT DATES**  
Paper Submission: 11 October 2023  
Workshop Proposals: 02 August 2023  
Panel Proposals: 13 December 2023  
Camera-Ready: 15 February 2024
3. IEEE Consumer Communications & Networking Conference  
6–9 January 2024 // Las Vegas, NV, USA  
**IMPORTANT DATES**  
Technical Papers due: 3 July 2023  
Acceptance Notification: 30 September 2023
4. IEEE International Conference on Computer Communications  
20–23 May 2024 // Vancouver, Canada  
**IMPORTANT DATES**  
Abstract Due:  
Monday, July 24, 2023 (11:59pm AOE)  
Full Paper Due: Monday, July 31, 2023 (11:59pm AOE)  
Notification of Acceptance: Friday, December 1, 2023
5. IEEE/IFIP Network Operations and Management Symposium  
6–10 May 2024 // Seoul, South Korea  
**IMPORTANT DATES**  
Paper Submission Deadline: Sep. 29, 2023  
Notification of Acceptance: Dec. 22, 2023  
Final Camera Ready: Feb. 2, 2024
6. (ICASSP 2024) 2024 IEEE International Conference on Acoustics, Speech and Signal Processing  
Date: 14–19 April 2024  
Location: Seoul, Korea
7. (CAI 2024) IEEE Conference on Artificial Intelligence  
Date: 25–27 June 2024  
Location: Sands Expo & Convention Ctr., Singapore  
Conference Paper Submission Deadline: December 01, 2023
8. (ICIP 2024) 2024 IEEE International Conference on Image Processing  
Date: October 27–30, 2024  
Location: Abu Dhabi, UAE  
Conference Paper Submission Deadline: TBA
9. 2023 IEEE International Conference on Microwaves, Communications, Antennas, Biomedical Engineering and Electronic Systems  
Date: 6 November 2023 – 8 November 2023
10. 2023 IEEE International Radar Conference  
Date: 6 November 2023 – 10 November 2023
11. 2024 International Radar Symposium  
Date: 2 July 2024 – 4 July 2024  
Geographic Location: Wroclaw, Poland

## CALL FOR PAPERS:

**LABTALK** is an in-house journal of CRL-Bengaluru. LABTALK is intended to provide a forum for CRL scientists to share and publish their novel research work and technology developments. Papers based on theoretical research, design, development and experimental work are published in LABTALK. Articles on new technology modules completed or under development are also brought out in LABTALK.

Original contributions are invited from CRL scientists for the upcoming LABTALK edition. The last date for submission of papers is 15th August 2023.

Further correspondence regarding paper format and design template will be communicated through mail.

Contact committee members for any clarifications.



Labtalk committee members with CS CRL-BG.

From left: Sayantan Mukherjee, Muhammed Ajeer VK, Dr Viji Paul P, Shri. L. Ramakrishnan, Santosh Kumar, Neelabh Keshav and Sapta Girish Babu Neelam.